Macromolecular Research
https://doi.org/10.1007/s13233-025-00475-7

ARTICLE

α-Aminophosphonates-functionalized poly(*p*-Hydroxystyrene): synthesis, characterization, DFT simulations, assessment of their antimicrobial and anticancer efficacy

Esraa M. El-nshar[1] · El-Refaie Kenawy[2] · Wesam E. Yousuf[3] · Ahmed R. Ghazy[4] · Kamal I. Aly[5] · Samar A. Khattab[2]

Received: 13 August 2025 / Revised: 1 November 2025 / Accepted: 5 November 2025

Abstract

α-Aminophosphonate and their related derivatives have garnered significant attention as a result of their use in many biological and industrial applications, particularly in the fields of materials science. This research described synthesis and characterization of novel α-aminophosphonate derivatives (ES1-ES4) based on poly(*p*-hydroxystyrene). The synthesis was achieved by chemically modification of poly(*p*-hydroxystyrene) (PHS) with triphenylphosphite and various aldehydes (vanillin, *N,N'*-dimethylaminobenzaldhyde, *p*-chlorobenzaldhyde, and 3,4,5-trimethoxybenzaldhyde). The chemical structures were confirmed using FT-IR, ^{1}H, ^{13}C and ^{31}P-NMR besides the thermal analysis techniques. A significant increase in molecular weight and radius of gyration were observed following functionalization, as evidenced by static laser light dispersion. The degree of functionalization (DoF) ranged from 71.5 to 80.06. The electronic properties and physical characteristics of these derivatives were elucidated through computational studies that employed DFT simulations. These studies revealed significant changes in the electron density distribution, electrostatic potential, and key polymeric properties, such as optical characteristics, mechanical strength, and glass transition temperature. Based on antimicrobial investigation, ES1 and ES4 showed potent inhibition against gram-positive bacteria and *Candida albicans*, indicating broad-spectrum activity. With a selectivity index of 1.50–1.72, cytotoxicity evaluations demonstrated that derivatives coded ES2, ES3, and ES4 exhibited reduced toxicity towards normal lung fibroblasts, recording IC_{50} of 181.37, 193.38 and 203.95 µg/mL, respectively. On the other hand, higher selective toxicity against HepG2 liver cancer cells with IC_{50} values: 118.27, 121.75 and 121.18 µg/mL. These results demonstrated that α-aminophosphonate hybrid polymers have great promise as antibacterial and preliminary anticancer potential against HepG2 cells, while maintaining moderate safety toward normal fibroblasts at lower concentrations.

✉ Esraa M. El-nshar
esraa.saad@su.edu.eg

El-Refaie Kenawy
ekenawy@yahoo.com

Wesam E. Yousuf
wessam-pg147370@science.tanta.edu.eg

Ahmed R. Ghazy
ahmed.ghazy@science.tanta.edu.eg

Kamal I. Aly
Kamalaly@aun.edu.eg

Samar A. Khattab
samar.khattab@science.tanta.edu.eg

[1] Chemistry Department, Faculty of Biotechnology, Sinai University, Kantara 41636, Egypt

[2] Polymer Research Group, Chemistry Department, Faculty of Science, Tanta University, Tanta 31527, Egypt

[3] Biochemistry Division, Chemistry Department, Faculty of Science, Tanta University, Tanta 31527, Egypt

[4] Laser Laboratory, Physics Department, Faculty of Science, Tanta University, Tanta 31527, Egypt

[5] Polymer Research Laboratory, Chemistry Department, Faculty of Science, Assiut University, Assiut 71516, Egypt

Published online: 15 December 2025

Graphical abstract

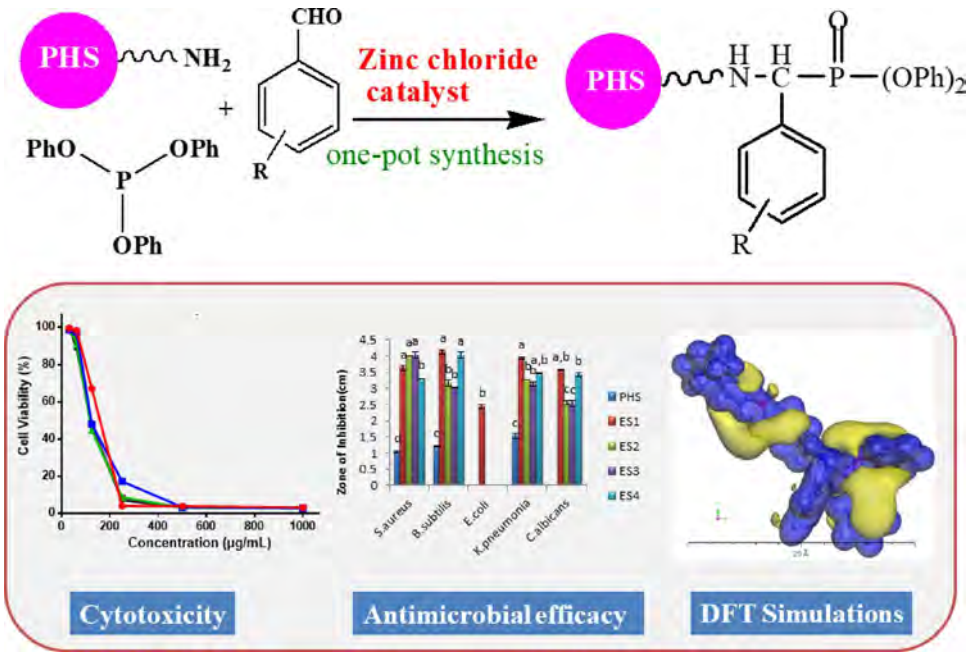

Keywords α-Aminophosphonates · Polyhydroxystyrene · DFT calculation · Anticancer · Antibacterial activity

1 Introduction

Novel polymeric systems provide significant opportunities for improving pharmaceutical technology in the management of health problems such as malignant tumors, acute immunodeficiency, diabetes and ischemia. Recently, researchers have focused on developing biodegradable polymers and exploring their potential in innovative therapeutic designs. Polymers containing phosphorus ester repeating units in the backbone that are known as aminophosphonates represent a privileged class in organophosphorus chemistry [1]. Because of their great biological efficiency, metabolic stability, and little toxicity to living cells, they have significance in drug design because they can break down into environmentally friendly constituents under physiological conditions [2]. The reactive functional groups in the backbone of these polymers allow bioactive ingredients to conjugate to their chains, opening up an extensive range of opportunities for the creation of novel medications with enhanced therapeutic index. The numerous biological activities of amino phosphoric acid derivatives are widely recognized [2, 3].

α-aminophosphonates exhibited several pharmacological activities as antibiotics, anti-thrombotic, inhibitors of HIV protease, anti-cancer agents, anti-inflammatory, anti-tubercular, catalytic antibodies, anti-oxidants, anti-microbial, herbicides, anti-viral agents and carriers of hydrophilic organic molecules across the phospholipid membranes [4–7].

Since the original synthesis in 1952, numerous techniques for producing various α-aminophosphonates have been reported [8]. The Kabachik-Fields (phospha-Mannich) method, which involves the three-component condensation of an amine, a carbonyl molecule, and diethylphosphite or triethylphosphite, is one of the most popular and widely used methods for the synthesis of α-aminophosphonate derivatives [9]. Lewis acid catalysts and/or solvents are usually used in these reactions, which maintain to be the most effective, straightforward, widespread, and high-yielding technique. The nature of reactants influences the reaction's mechanism. It has been proposed that an imine or α-hydroxyphosphonate may be employed as intermediates during the condensation. However, a number of these techniques have certain disadvantages, including long reaction periods, poor product yields, the need for stoichiometric quantities of catalysts, expensive and moisture-sensitive catalysts, and the use of extremely toxic or hazardous catalysts [10].

In previous work, Al-Jubori et al. [11] synthesized Benzo[d]imidazole α-aminophosphate derivatives with one-pot reaction of magnesium triflate as a catalyst that evaluated their activities against microbial drug-resistance species. Mungara et al. [12] synthesized carbazole-based

α-aminophosphonates and evaluated their antiproliferative activity.

Polymers bearing α-aminophosphates moieties are a promising class of biologically active polymers [13, 14]. The biological activities of a variety of polymers, including chitosan, cellulose, and derivatives of acrylic acid, have been investigated [15]. Among the many synthetic polymers used in the biomedical fields is poly (*p*-hydroxystyrene) (PHS). Several studies have reported the biological effect of PHS as in Kenawy et al., which studied the antimicrobial effects of the cationic ammonium and phosphonium salts of poly (*p*-hydroxystyrene) [16]. The presence of reactive hydroxyl groups (-OH) in the PHS side chain allows for its modification into numerous derivatives, thereby expanding its applications in the biomedical field [17].

Recently, our research group studied the synthesis of polyhydroxystyrene and their anticancer activities were studied [18]. Thus, as a part of our continuing studies in synthesis of biologically active polymers, new series of polymers bearing α-aminophosphonates moieties have been synthesized. To our knowledge, the α-aminophosphonates derived from poly (*p*-hydroxystyrene) have not been studied yet.

The aminophosphonates derivatives were designed via the reaction of aminated polyhydroxystyrene with various aldehydes and triphenylphosphite in the presence of zinc chloride as a catalyst. The obtained aminophosphonates were tested for their antibacterial and antitumor activities.

2 Experimental

2.1 Materials

Linear poly(*p*-hydroxystyrene) (PHS) was purchased from TriQuest, LP, A ChemFirst Company. Chloroacetylchloride, pyridine, Dimethyl sulfoxide (DMSO), nutrient agar, Sabouraud dextrose agar, nutrient broth and Sabouraud dextrose broth were purchased from El-Nasr pharmaceutical chemicals, Egypt. Ethylenediamine, triphenylphosphite, Vanillin, *N*,*N*'-dimethylaminobenzaldhyde, *p*-Chlorobenzaldhyde, 3,4,5-trimethoxybenzaldhyde, MTT [3(4,5-dimethylthiazol-2-yl)-2,5-diphenyltetrazolium bromide] and phosphate-buffered saline (PBS) were supplied from Sigma-Aldrich, (USA). Zinc chloride was supplied from Thermo Scientific Chemicals (USA). Dimethylformamide (DMF), diethylether and methylene chloride were supplied from El- Gomhouria chemicals company, Egypt. RPMI medium supplemented with 2% serum as a maintenance medium.

2.2 Characterization techniques

FT-IR spectral data were recorded on Perkin Elmer 1430 ratio using KBr pellets within the wavelength range of 400–4000 cm^{-1}. Thermogravemetric analysis (TGA) and Differential thermogravimetric (DTG) were carried out on Perkin Elmer TGA 4000 Thermogravimetric analyzer using 5–10 mg of tested polymer and scanned from 40 to 800 °C at a rate of 30 °C/min covered with N_2 with a flow rate of 20 mL/min. NMR spectra were captured on a Varian Mercury 400 NMR Spectrometer using TMS as an internal reference and deuterated DMSO as a solvent.

2.3 Synthesis of chloroacetylated poly(*p*-hyroxystyrene)

Chloroacetylated PHS was prepared as previously described in our work [19]. Briefly, pyridine (8 mL) was added to a solution of poly(*p*-hyroxystyrene) (8 g, 66.67 mmol) dissolved in 60 mL DMF, Afterwards, Chloroacetylchloride (8 mL, 100.44 mmol) was added dropwise to the cold reaction mixture. The mixture was then allowed to proceed at room temperature for three days. After precipitating in 1N HCl, the product was filtered and repeatedly purified with distilled water. The product was coded as (Cl-PHS).

2.4 Modification of chloroacetylated poly(*p*-hyroxystyrene) with ethylenediamine

In a 100 mL round-bottomed flask containing ethylenediamine (EDA) (2 mL, 33.2 mmol), Cl-PHS (0.32 g, 1.17 mmol) dissolving in 20 mL DMF was added. The mixture was refluxed for 4 days at 80 °C, then the product was precipitated in hot water and washed with diethylether. The polymer was coded as (NH_2-PHS).

2.5 General procedures for synthesis of α-aminophosphonate based on poly(*p*-hydroxystyrene)

Aminated PHS (2.26 mmol) and different aldehydes (2.7 mmol) were stirred in 10 mL methylene chloride, then triphenylphosphite (2.26 mmol) and 10 wt% of anhydrous zinc chloride $ZnCl_2$ were added. The reaction mixture was stirred for 24 h at ambient temperature. The product was obtained by precipitation in distilled water then recrystallized to obtain a pure product. The obtained modified polymers were coded as (ES1-ES4).

2.6 Antimicrobial activity assessment

The agar well diffusion technique was applied to assess the antibacterial effect of PHS and its derivatives (ES1, ES2, ES3 and ES4 [20]. The test microorganisms utilized in this study were sourced from the Department of Microbiology, Faculty of Science, Tanta University, Egypt. The pathogenic strains comprised Gram-positive bacteria, including *Staphylococcus aureus (ATCC 25923)* and *Bacillus subtilis (ATCC 6633)*, Gram-negative bacteria such as *Escherichia coli O157 (KY797670)* and *Klebsiella pneumoniae (ST627)*, in addition to the fungal strain *Candida albicans (ATCC 10231)*. Each strain of bacteria was stored on nutrient agar slants at 4 °C [21], while *C. albicans* was preserved on Sabouraud dextrose agar [22]. Before testing, the bacterial cultures were cultivated in nutritional broth at 37 °C for 24 h, while the fungal culture was cultivated in Sabouraud dextrose broth at 28 °C for 48 h [23]. The microbiological suspensions were calibrated to conform to the 0.5 McFarland standard (about 1.5×10^8 CFU/mL for bacteria and 1.5×10^6 CFU/mL for fungus) [24]. The parent polymer (PHS) and its derivatives, aminophosphonate compounds ES1, ES2, ES3, and ES4, were dissolved at a concentration of 10 µg/mL in DMSO to create stock solutions [25]. To find the minimal inhibitory concentration (MIC), serial dilutions of 10, 5, 2.5, 1.25, and 0.625 µg/mL were made [26]. The broth dilution method was used to calculate the minimum inhibitory concentration (MIC) [27]. The relatively low MIC concentration range applied in this study (10–0.625 µg/mL) was selected based on preliminary inhibition zone results, which indicated that the tested α-aminophosphonate derivatives exerted strong antibacterial effects even at low doses. The use of such a narrow concentration gradient allows for a more precise estimation of minimal inhibitory levels and is consistent with earlier reports describing high potency of organophosphorus and cationic polymeric compounds against Gram-positive and Gram-negative strains at comparable microgram ranges [28]. Differences between antibacterial and cytotoxicity test concentrations are therefore attributed to the higher resistance of mammalian cells to polymeric materials compared with microbial cells. Each study was carried out in triplicate, and the mean ± standard deviation (SD) was used to express the results.

2.7 In vitro anti-proliferative activity

2.7.1 Cell lines and culture conditions

The National Cancer Institute (Cairo, Egypt) provided the HepG2 (human hepatocellular carcinoma) and WI38 (normal human lung fibroblasts) cell lines. The cells were cultivated at 37 °C in a humidified environment with 5% CO_2 in Roswell Park Memorial Institute medium (RPMI) supplemented with 2% serum [29].

2.7.2 Cytotoxicity assessment

The cytotoxic effects of PHS and its derivatives (ES1, ES2, ES3 and ES4) were evaluated using the MTT assay [30]. After being seeded at a density of 1×10^5 cells/mL in 96-well culture plates, the cells were left to form a monolayer for 24 h. The cells were treated with two-fold serial dilutions of the test substances (31.25–1000 µg/mL) following monolayer washing. Only the maintenance medium was given to the control wells. Following a 24-h treatment period, 100 µl of cell suspension was added to each well, along with 10 µl of MTT solution (5 mg/mL in PBS). After incubating for four hours, the formazan crystals were dissolved in 200 µl of DMSO after the supernatant was carefully removed. A microplate reader was used to measure the absorbance at 620 nm. To ensure that the observed responses were solely attributed to the synthesized compounds, the DMSO concentration in all experiments was kept below 0.5% v/v, which is generally considered non-toxic under MTT assay conditions. A vehicle control containing the same DMSO level was included in each plate to exclude solvent-induced effects. Cell viability was reported as a percentage in relation to the control, and untreated control wells were added under the same circumstances. The percentage of cell viability was determined using the formula below:

(Mean O.D. of treated cells/Mean O.D. of control cells) × 100 = cell viability (%) [31]. The cytotoxicity percentage was determined using the equation:

$$\text{Cytotoxicity } (\%) = 100 - \text{ Cell viability } (\%)$$ [32].

The IC_{50} values were calculated using GraphPad Prism software (version X) through nonlinear regression analysis of the dose–response curves. The cytotoxicity evaluation against mammalian cells was carried out at higher concentrations (31.25–1000 µg/mL) to accurately determine IC_{50} values. This approach is commonly adopted because mammalian cells are generally more tolerant to polymeric materials than microbial cells, requiring higher doses before significant cytotoxicity is observed. Similar observations have been reported for various polymeric antimicrobial systems, where effective antibacterial activity was achieved at 10 of µg/mL, whereas cytotoxic responses in mammalian cells appeared only above several 100 µg/mL [33, 34]. The selectivity index (SI) of the compounds was calculated according to the following formula:

$$SI = IC_{50}\,(Wi38)\,/IC_{50}\,(HepG2)$$ [35].

2.7.3 Morphological analysis

Cellular morphological alterations were analyzed with a phase contrast inverted microscope. Structural alterations in both WI38 and HepG2 cells were examined after a 24-h exposure to varying doses of the test substances. Alterations in cell surface characteristics and cytoskeletal configurations were recorded and associated with cell viability metrics [36].

2.8 Statistical analysis

The variations in inhibition zones were examined using one-way analysis of variance (ANOVA). To find statistically significant differences between samples, a post hoc analysis using Duncan's multiple range test was performed. *P*-values below 0.05 were regarded as statistically significant.

3 Results and discussion

Synthesis of *α*-aminophosphonate derivatives [ES1-ES4] was followed the route as illustrated in scheme 1, where the aminated polymer and different aldehydes as Vanillin, *N,N'*-dimethylaminobenzaldhyde, *p*-chlorobenzaldhyde and 3,4,5-trimethoxybenzaldhyde were reacted with triphenylphosphite in the presence of zinc chloride as catalyst. The chemical structures of α-aminophosphonates were confirmed by FTIR, ^{1}H NMR, ^{13}C NMR, ^{31}P NMR and TGA.

3.1 Chemical characterization

The FTIR spectra of poly(*p*-hydroxystyrene) and its modifications are presented in Fig. 1. Compared to the pristine PHS, the chloroacetylated PHS's FTIR spectrum displayed new peaks at 1729 and 1656 cm^{-1}, which indicated the

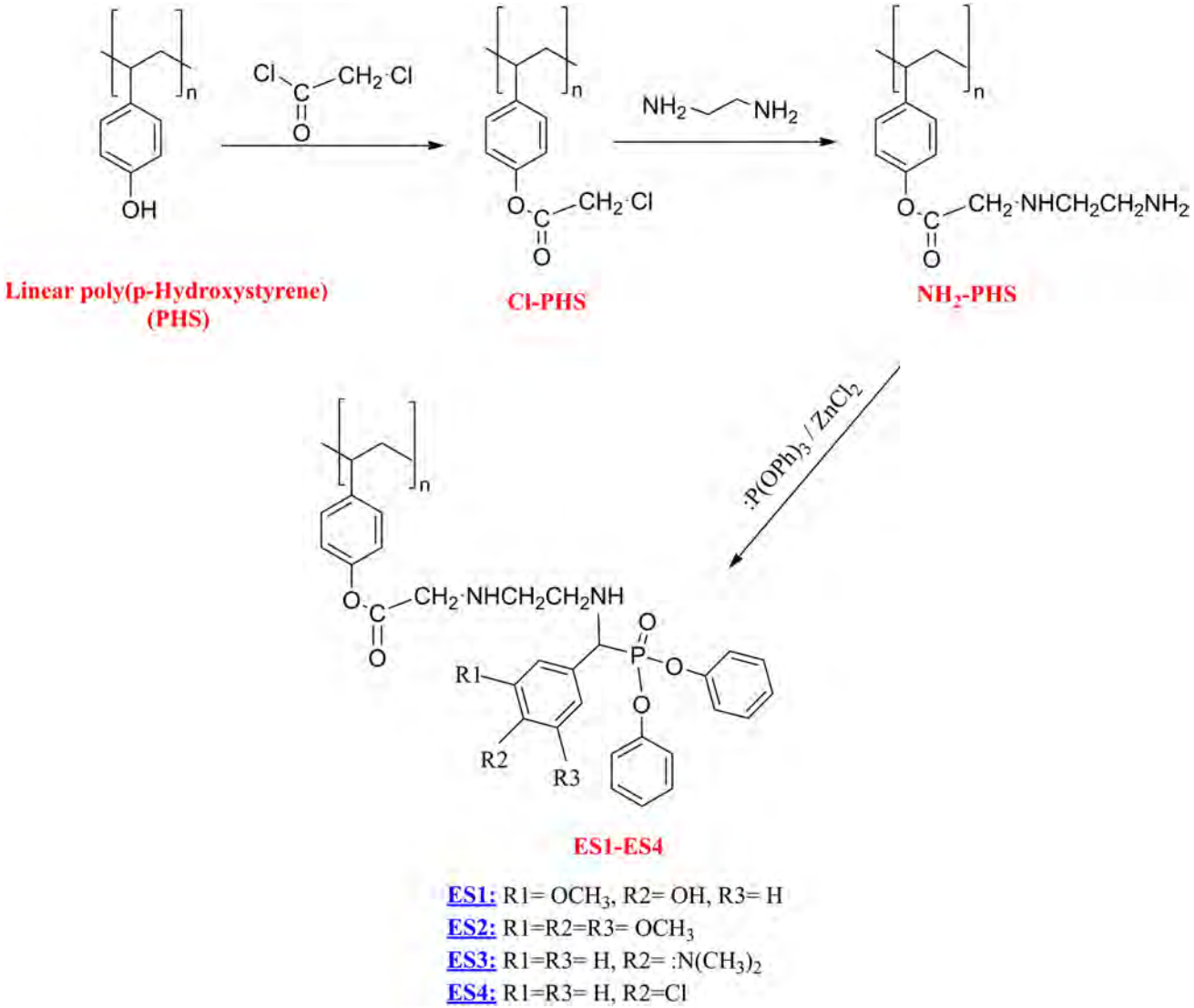

Scheme 1 Synthesis of α-aminophosphonates derived from poly(*p*-hyroxystyrene)

presence of a C=O group in the acetyl group. The aminated polymer spectrum showed a peak at 3354 cm^{-1}, attributed to the stretching of terminal amino groups and the peak for C=O was shifted due to the near amino that strengthen the band at 1655 cm^{-1} and the band at 1513 cm^{-1} indicated the presence of N–H secondary amine. The FTIR spectral analysis of α-aminophosphonate derivatives (ES1-ES4) showed broad absorption bands at the range of 3500–3573 cm^{-1} for NH stretching and at 1600–1013 cm^{-1} for NH bending. Absorption bands in the 1218–1234 cm^{-1} region appeared due to the stretching vibration of P=O, a new band around 1100 cm^{-1} appeared for P-O-C stretching, while the bands at 950 cm^{-1} were referred to P–C [37, 38].

The NMR results further manifested the structure of aminophosphonate polymers. For ES1: ^{1}H NMR: δ 1.2– 1.7 (d, *J=6.7 Hz*, 2H, C$\underline{H}_2$ in the main polymer backbone), 2.47 – 2.53 (m, 1H, C$\underline{H}$-CH_2 in polymer backbone), 3.54 (s, 4H, C$\underline{H}_2$NH), 3.69 (s, *J=6.5 Hz,* 2H, COC$\underline{H}_2$), 3.83 (s, 3H, O-C$\underline{H}_3$), 5.9 (s, 1H, O$\underline{H}$), 6.3 –6.5 (m, 4H, C_6H_5), 7.19 – 7.10 (m, 3H, C_6H_5),7.45 – 7.36 (m, 10H, C_6H_5), 6.75 (dd, 1H, C$\underline{H}$P). ^{13}C NMR (101 MHz, DMSO-d6) δ 191.53 (C=O), 157.04, 155.40, 153.48, 148.62, 147.88, 146.31, 130.94, 130.86, 130.17, 129.85, 128.57, 126.55, 125.51, 120.86, 119.29, 116.04, 115.86, 115.83, 115.69, 115.34, 111.17 ($C_{Aromatic}$), 68.22 (O$\underline{C}H_3$), 56.11 (C$\underline{H}$P), 34.88 (CO$\underline{C}$H), 30.92 (NH$\underline{CHCH}$NH), 19.58 ($CH_{aliphatic}$ in polymer backbone). ^{31}P NMR (162 MHz, DMSO-d6) δ 19.93.

For ES2: ^{1}H NMR: δ 0.89 (d, *J=6.7 Hz*, 2H, C$\underline{H}_2$ in the main polymer backbone), 3.71 (d, *J=6.6 Hz*, 2H, COC$\underline{H}_2$), 3.77 (s, 3H, OC$\underline{H}_3$), 3.86 (s, 6H, OC$\underline{H}_3$), 3.64 (d, J=9.3 Hz, 4H, C$\underline{H}_2$NH), 6.76 (d, *J=*8.2 Hz, 1H, C$\underline{H}$P), 6.94 (s, 2H, C_6H_5), 6.85 (d, *J=9.4 Hz*, 3H, C_6H_5), 7.38 – 7.24 (m, 10H, C_6H_5) .^{13}C NMR (101 MHz, DMSO-d6) δ 192.40 (C=O), 153.81, 153.25, 132.13, 130.96, 130.23, 130.12, 128.57, 125.50, 120.81, 120.76, 115.91, 115.17, 107.22 ($C_{Aromatic}$), 60.71 (O$\underline{C}H_3$), 60.51 (C$\underline{H}$P), 56.54 (CO$\underline{C}$H), 56.34 (NH$\underline{CHCH}$NH). ^{31}P NMR (162 MHz, DMSO) δ 19.35.

For ES3: ^{1}H NMR: δ 1.80 (d, *J=170.8 Hz*, 2H, CH_2 in the main polymer backbone), 3.77 (s, 4H, C$\underline{H}_2$NH), 2.79 (p, J=1.8 Hz, 6H, N(C$\underline{H}_3$)$_2$), 3.20 (d, *J=9.7 Hz*, 2H, COC$\underline{H}_2$), 6.79 (s, 1H, C$\underline{H}$P), 7.98 (m, 10H, 2 Ph-O), 7.68 – 7.52 (m, 2H, C_6H_5), 7.16 – 7.01 (m, 4H, C_6H_5). ^{13}C NMR (101 MHz, DMSO) δ 190.34 (C=O), 154.68, 132.02, 130.84, 130.52, 130.43, 130.32, 130.16, 130.14, 128.58, 125.48, 125.00, 120.88, 120.84, 115.82, 115.18, 111.54 ($C_{Aromatic}$). ^{31}P NMR (162 MHz, DMSO) δ 21.60.

For ES4: ^{1}H NMR: δ 1.50 (d, *J=*162.1 Hz, 2H, CH_2 in the main polymer backbone), 2.55 (t, *J=*5.4 Hz, 1H, C$\underline{H}$-CH_2 in polymer backbone), 3.18 (s, 2H, COC$\underline{H}_2$), 3.41 (s, 4H, C$\underline{H}_2$NH), 5.47 (d, *J=*12.6 Hz, 1H, C$\underline{H}$P), 7.73 – 7.52 (m, 1H, C_6H_5), 7.45 (m, *J=*8.6 Hz, 1H, C_6H_5), 7.39 – 7.24 (m, 3H, C_6H_5), 7.22 – 7.00 (m, 5H), 6.86 (d, *J=*8.6 Hz, 1H), 6.80 – 6.66 (m, 4H). ^{13}C NMR (101 MHz, DMSO) δ 192.59 (C=O), 157.76, 156.12, 155.39, 134.63, 131.14, 130.75, 130.44, 130.30, 130.28, 129.94, 129.85, 128.60, 128.57,

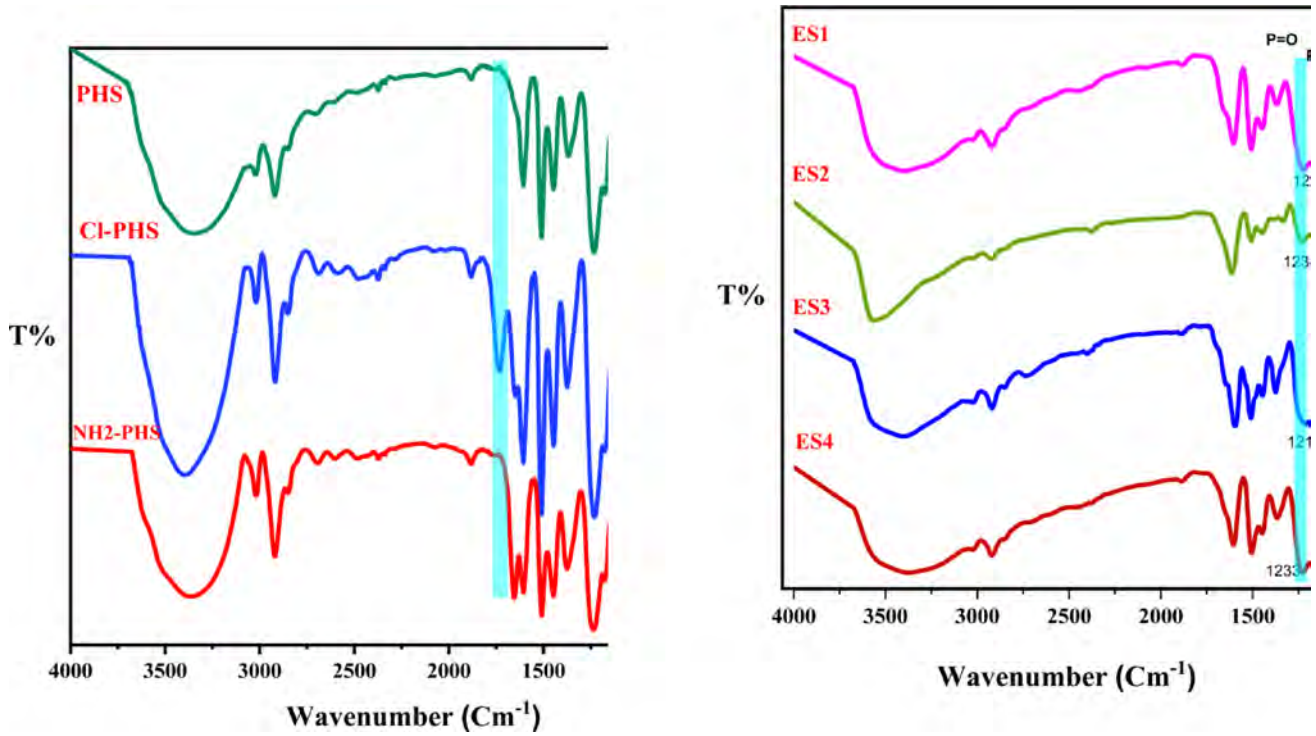

Fig. 1 FTIR spectra of poly(*p*-hydroxystyrene) and its modifications

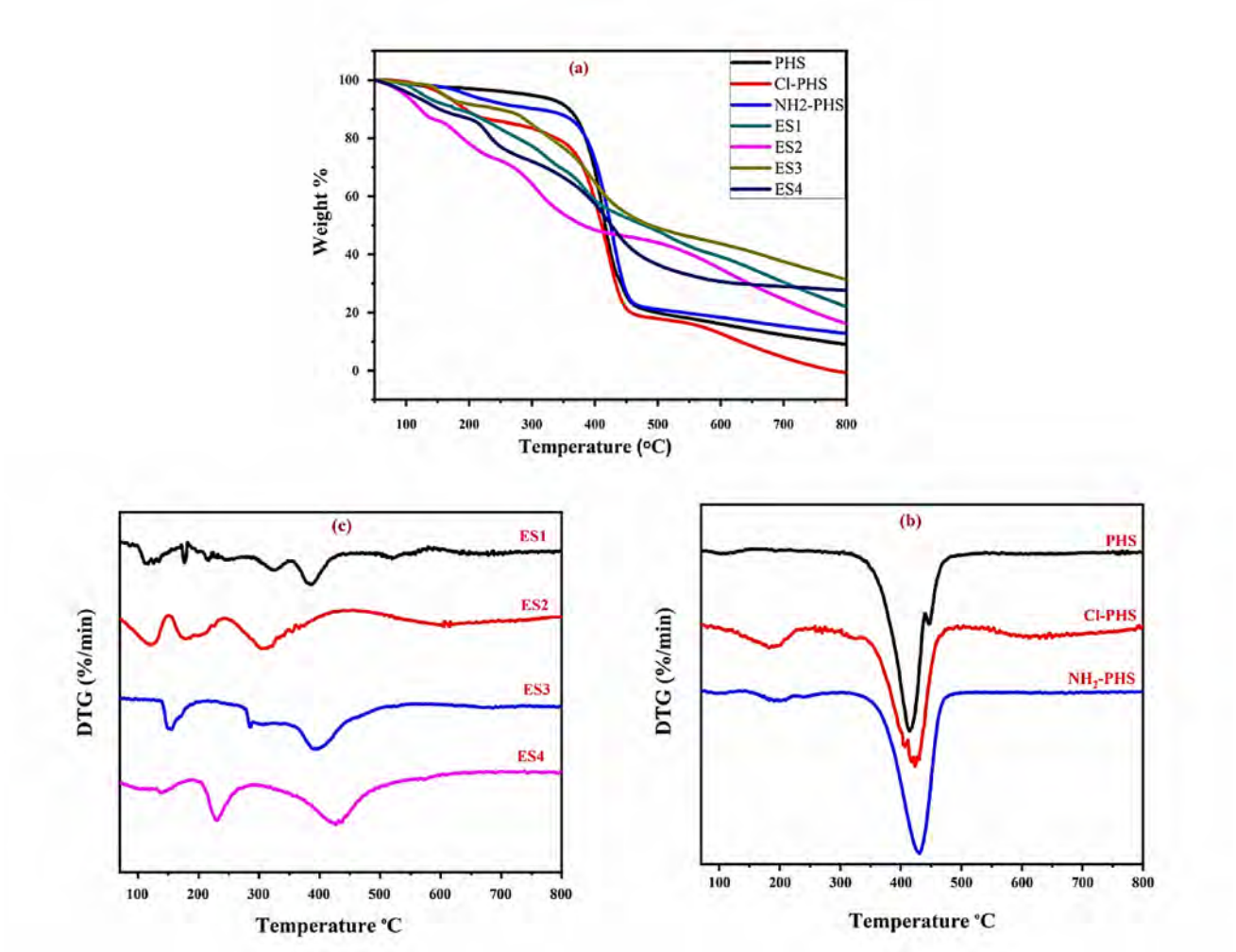

Fig. 2 **a** TGA curves **b** and **c** DTG curves of poly *p*-hydroxystyrene and its modifications

Table 1 TGA data of poly(*p*-hydroxystyrene) and its modifications

Code	T_{onset}	$T_{-50\%}$	% Total Wt. loss
PHS	373	416	90
Cl-PHS	351	409	100
NH_2-PHS	363	424	87
ES1	170	474	77
ES2	156	380	83
ES3	143	489	68
ES4	204	426	72

128.53, 125.63, 125.59, 120.93, 120.89, 120.85, 120.76, 119.29, 115.70, 115.56, 115.19 ($C_{Aromatic}$), 69.95 (CHP), 68.31 ($CO\underline{C}H_3$), 63.27 (NHCHCHNH), 54.07 ($CH_{aliphatic}$ in polymer backbone). ^{31}P NMR (162 MHz, DMSO) δ 15.21 [39, 40].

The thermal characteristics of the polymers were established using TGA and DTG as shown in Fig. 2a, b and c, respectively. The chemical structure and intra- and intermolecular forces of a molecule determine its thermal stability. The temperatures at which the first breakdown took place (T_{onset}), 50% weight loss happened ($T_{-50\ wt\%}$), and the total weight loss were listed in Table 1. The thermal degradation of the pristine PHS, Cl-PHS and NH2-PHS exhibited similar patterns of weight loss degradation. In the beginning, there was a weight loss of 3% below 150 °C due to the removal of bound water molecules and moisture. Pristine polymer (PHS) started to degrade at 373 °C losing 65% of its weight at 475 °C which could be attributed to the degradation of polymer chains [41]. TGA of both Cl-PHS and NH2-PHS displayed initial weight loss earlier than the pristine PHS due to the incorporation of hydrophilic moieties such as chloroacetylchloride and amino groups. The onset temperature of chloroacetylated polymer was at 351 °C and the aminated one was at 363 °C. Cl-PHS displayed weight loss of 14% in the range of (140–234 °C), this revealed that the substitution degree of the hydroxyl group with the chloroacetyl group was 36%. NH_2-PHS started to decompose and lost 14% of its weight in the range of 174–373 °C due to the decomposition of amine moieties. According to this, the

degree of amination was estimated as 52%. Similar results were reported by Morshedy et al. [42]. On the other hand, the TGA patterns of the four aminophosphonates (ES1-ES4) were different compared to the unmodified polymer, which displayed multi-steps of degradation as shown in DTG curves (Fig. 2c). Polymer (ES3), which contains dimethylaminobenzaldehyde moieties revealed the highest thermal stability among other derivatives leaving a residual weight of 32%.

3.2 Static light scattering

Static laser light scattering was used to measure the second virial coefficient (A), radius of gyration (R_g), and polymer molecular weight (M_w). A high-precision Abbe digital refractometer was used to quantify the refractive index increment (dn/dc), which is an essential metric for examining polymer–solvent interactions at various polymer concentrations[40,41]. The increment in refractive index was calculated using the formula [43, 44]:

$dn/dc|_{c\to 0} = \underset{c\to o}{\mathrm{Lim}}\,(n - n_o/c)$, where c, n_o, and n represent concentration, solvent, and solution refractive indices, respectively.

The samples' dn/dc values differed greatly from one another, ES2 had the highest value (3.2662 mL/g), suggesting that there was more light scattering because of the higher molecular interactions. The generated concentrated scattered light intensity angular distribution was assessed between 40° and 140° using an Oriel photomultiplier tube type 77,344 [Fig. 3a–e]. A 650 nm Nd-YAG laser was the source of the incident light.

Using the basic Rayleigh scattering equation, the computed scattering parameters for molecular weight (MW), radius of gyration (R_G), and second virial coefficient (A_2) are displayed in Zimm plot Fig. 4a–e [45–48].

$$\frac{Kc}{R_\theta} = \frac{1}{M_w}\left[1 + \left(\frac{16\pi^2}{3\lambda^2}\right) R_G^2 \sin^2\left(\frac{\theta}{2}\right)\right] + 2A_2c$$

where $K = 2\pi^2 n_o^2/\lambda^4 N_A (dn/dc)^2 \left(1 + \cos^2\theta\right)$ and $R_\theta = I_\theta r^2/I_o V$.

Where λ is the wavelength of the scattered light, n_o is the solvent index of refraction, N_A is the number of Avogadro's, V is the scattering volume, θ is the scattering angle, and r is the distance between the scattering point and the detector. Table 2 displays a summary of the computed scattering parameter values and the refractive index increment. Following functionalization, the molecular weight (Mw), radius of gyration (Rg), refractive index increment (dn/dc), and second virial coefficient (A_2) all rose, indicating that PHS had been successfully modified. Strong polymer–solvent interactions are suggested by ES2's highest dn/dc value (3.2662 mL/g), whereas ES1's lowest value (1.859 mL/g) indicates lower solubility.

ES2 (71,740.4 g/mol)>ES4 (70,896.8 g/mol)>ES3 (70,230.8 g/mol)>ES1 (67,879.8 g/mol), indicating a considerable rise in M_w. A similar pattern was seen in the R_g values, indicating that polymer expansion was a result of functionalization. While ES1 had the lowest A_2, indicating

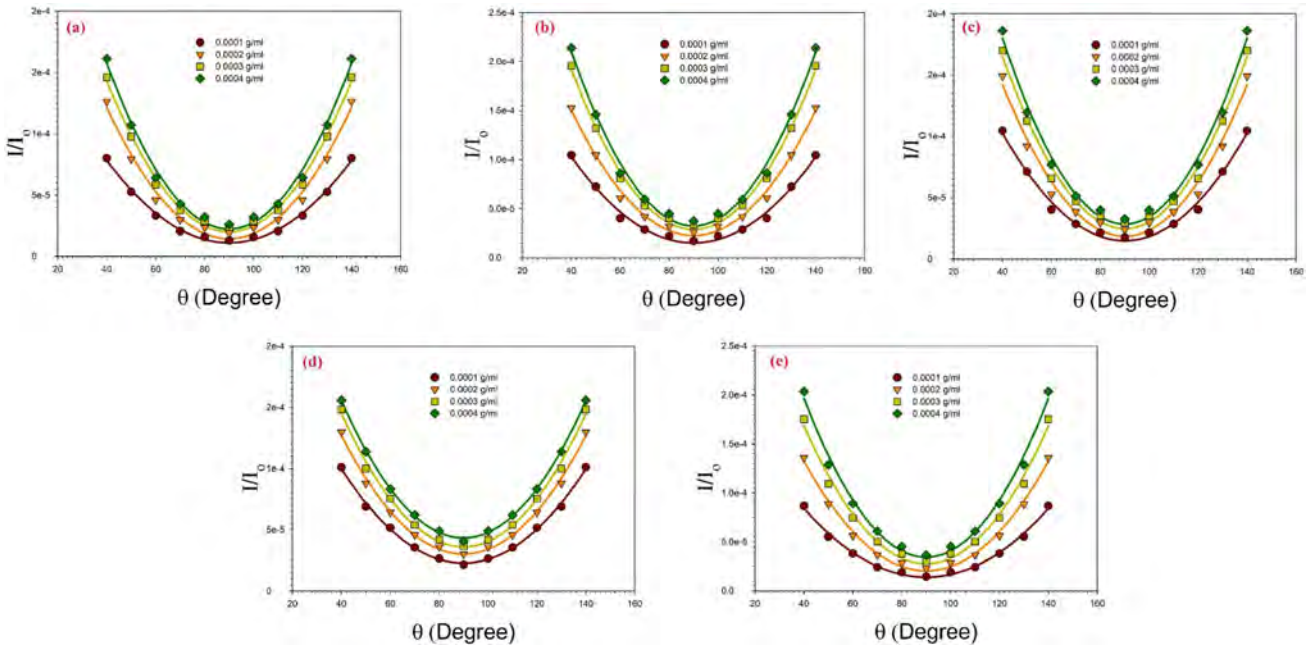

Fig. 3 Scattering angular distribution of **a** PHS, **b** ES1, **c** ES2, **d** ES3 and **e** ES4

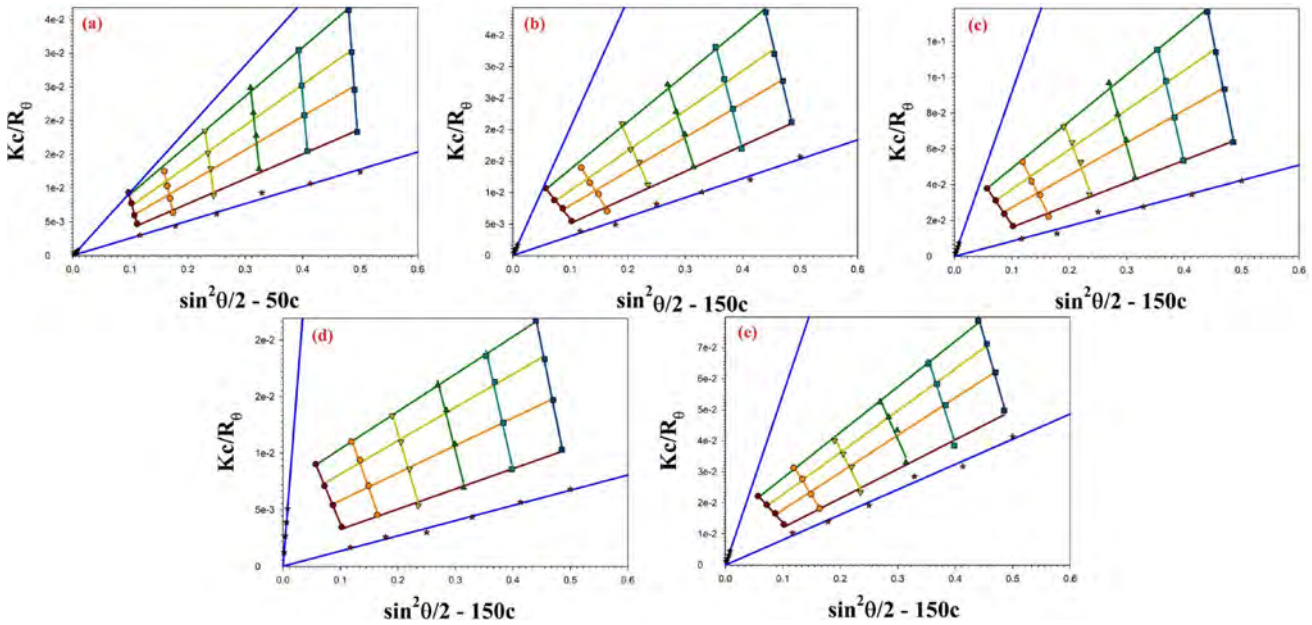

Fig. 4 Zimm plot of **a** PHS, **b** ES1, **c** ES2, **d** ES3 and **e** ES4

Table 2 Measured molecular weight, radius of gyration, second virial coefficient and degree of Degree of Functionalization of PHS and its modifications

	M_w (Fun. G)	dn/dc	M_w (g/mol)	R_g (μm)	A_2 (mol.cm^3/g^2)	DoF
PHS	–	1.507	34,305.6	2.65	0.942	–
ES1	469	1.859	67,879.8	4.08	2.032	71.5
ES2	513	3.2662	71,740.4	6.99	9.156	72.9
ES3	466	1.4573	70,230.8	2.75	6.435	77.09
ES4	457	2.613	70,896.8	6.79	5.485	80.06

steric hindrance, ES2 had the greatest, indicating the best solubility.

The molecular weight difference between the modified and unmodified polymers was used to measure the Degree of Functionalization (DoF), which is the number of functional groups added per polymer chain as follows:

$$DoF = \frac{M_w\,(modifiedpolymer) - M_w(PHS)}{M_w\,(functionalgroups)}$$

The values of Degree of Functionalization (DoF) and the molecular weight of the functional groups of each modification are listed in Table 2. Successful functionalization is confirmed by the DoF values, which show that ES4 had the highest (80.06) because of little steric hindrance and ES1 had the lowest (71.5) because of hydroxyl (-OH) interactions. Steric and electronic effects are reflected in DoF variations, with bulkier groups (ES2, ES3) displaying intermediate values. This implies that the samples' functionalization was effective yet varied.

3.3 TD-DFT simulations

The Local Density Approximation (LDA) functional in the TD-DFT/*DMol*^{3} module was used to model the electron density distribution for poly(*p*-hydroxystyrene) (PHS) and its derivatives (ES1–ES4) (Fig. 5). With its ability to effectively capture short-range exchange–correlation effects, the LDA technique offers a comprehensive knowledge of the charge distribution inside molecular structures [49, 50]. PHS shows a stable conjugated system with a well-localized electron density, mainly around the aromatic ring and hydroxyl groups, as shown in the electron density maps. ES1–ES4 exhibit notable electronic structural changes during functionalization, with the type of substituents having an impact on the redistribution of electron density. The inclusion of π-conjugated groups in ES1 and ES2 results in greater delocalization, while the addition of electronegative or electron-donating groups in ES3 and ES4 causes more polarized electron distributions. These electronic changes are well captured by the LDA functional, showing that substituent-induced changes can drastically change molecule reactivity and charge localization.

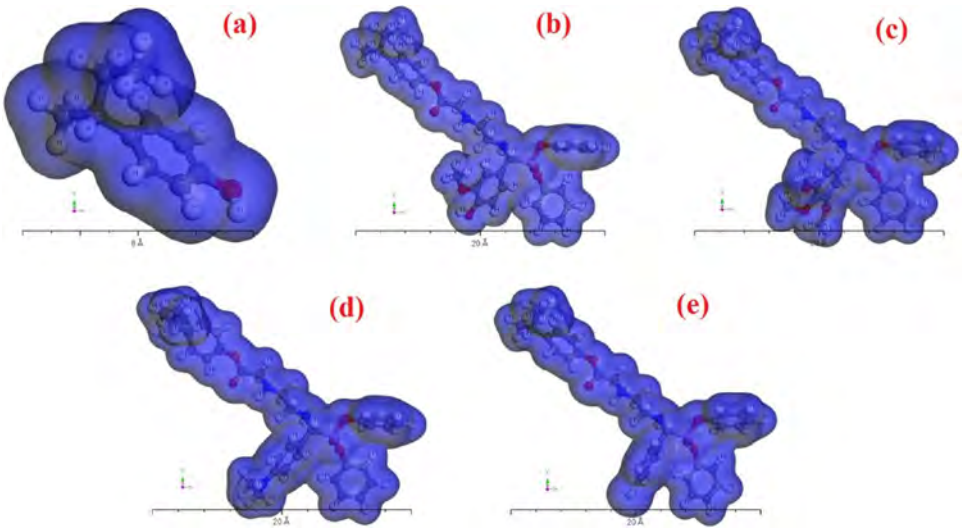

Fig. 5 Electron density of **a** PHS, **b** ES1, **c** ES2, **d** ES3 and **e** ES4

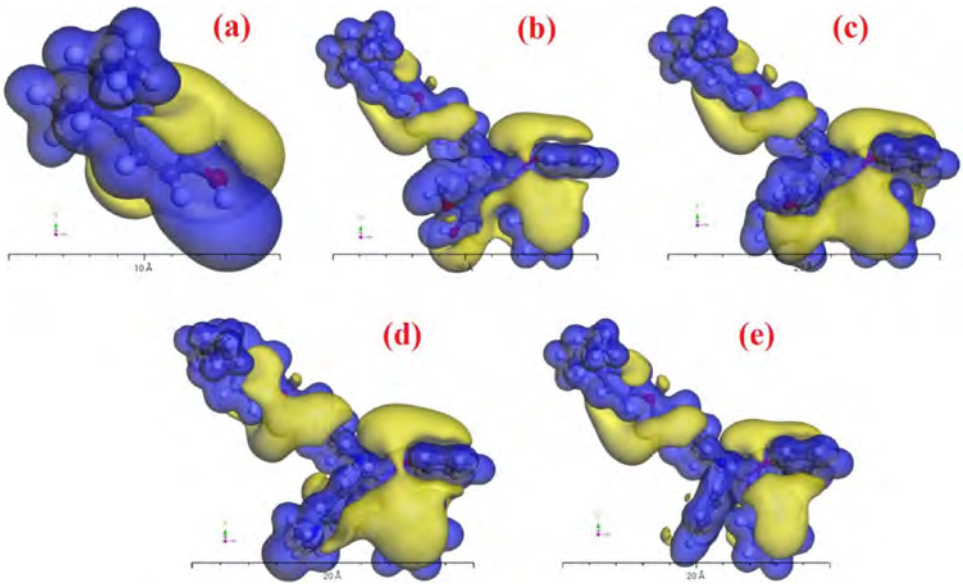

Fig. 6 electrostatic potential of **a** PHS, **b** ES1, **c** ES2, **d** ES3 and **e** ES4

The TD-DFT/*DMol*^{3} module with the Local Density Approximation (LDA) functional was used to analyze the distribution of electrostatic potentials (ESP) for PHS and its derivatives (ES1-ES4) (Fig. 6). The charge distribution across the molecular structures is shown by the ESP maps, where yellow regions denote locations with a positive potential and blue regions show areas with a negative potential, or electrons. The hydroxyl groups in PHS are highlighted as active locations for possible interactions by the significant negative potential that is seen surrounding them. When substituents are added, the system's electron-donating or electron-withdrawing properties change, resulting in substantial changes in the charge distribution in ES1–ES4. Conjugated systems in ES1 and ES2 lead to improved charge delocalization, whereas electronegative substituents in ES3 and ES4 provide greater localized electrostatic interactions.

Using the *Synthia* simulation module in DFT simulations at 298 ^{o}K, important polymeric physical characteristics were calculated for PHS and its derivatives (Table 3) [47, 51].

Because of the various functional groups bonded to the polymer backbone, the modified PHS derivatives (ES1–ES4) exhibit notable differences in their physical characteristics. From PHS (406.19 K) to ES derivatives, the glass transition temperature (T_g) drops, ES2 has the lowest T_g (368.10 K), most likely as a result of the methoxy (-OCH_3) groups that lessen intermolecular interactions. Comparing all derivatives to PHS, the molar volume also rises noticeably, suggesting that bulky substituents reduce packing efficiency and add free volume. According to the density trends, electron-donating groups in ES2 and ES3 decrease density, however the addition of chlorine (ES4) increases mass per unit volume. As predicted, the heat capacity (Cp) rises with molecular complexity, ES2 has the highest Cp

Table 3 Physical properties of PHS and its derivatives calculated using DFT/Synthia simulations at 298°K

Physical property	PHS	ES1	ES2	ES3	ES4
Glass transition temperature Tg (°K)	406.19	380.25	368.10	371.18	378.84
Molar volume	103.31	456.13	499.99	468.00	438.36
Density (kg/l)	1.162	1.253	1.231	1.215	1.277
Cp of solid (J kg^{-1} K^{-1})	151.43	693.84	755.48	701.48	653.87
Surface tension (Fedors) $N.m^{-1}$	54.84	48.08	44.35	44.27	45.88
Thermal conductivity W m^{-1} K^{-1}	0.14710	0.15326	0.15329	0.14970	0.14973
Refractive index	1.6084	1.5781	1.5676	1.5751	1.5841
Molar refraction $m^3.mol^{-1}$	35.74	151.39	163.48	154.69	146.73
Dielectric constant	3.333	3.339	3.203	3.149	3.189
Diamagnetic susceptibility	76.33	342.37	375.94	352.17	333.94
Bulk modulus (GPa)	5.794	4.559	3.950	3.963	4.239
Shear modulus (GPa)	1.889	3.713	3.371	3.270	3.378
Young's modulus (GPa)	5.113	8.762	7.873	7.694	8.008
Poisson's ratio	0.3529	0.1797	0.1677	0.1764	0.1851
Molar stiffness function ($N.m^{-2}$)	35.98	122.13	121.52	121.13	123.86

(755.48 J/kg·K), most likely because of its flexible ether groups, which aid in energy absorption. The reduced dipolar interactions from the tertiary amine may be the reason for the modest decrease in the dielectric constant in the substituted polymers, with ES3 having the lowest value (3.149). According to mechanical properties, ES1 (8.762 GPa) is the stiffest, indicating increased intermolecular contacts from hydrogen bonding, whereas PHS has a lower Young's modulus (5.113 GPa). On the other hand, ES2 and ES3 have lower bulk and shear moduli, which is consistent with their greater flexibility. The significance of large, electron-donating groups on decreasing polarizability is further supported by the fact that the optical characteristics, especially refractive index, drop in the ES derivatives as compared to PHS, with ES2 displaying the lowest value (1.5676). All things considered, these structural changes dramatically change the thermal, mechanical, and dielectric characteristics, showing that these polymers may be customized for certain uses like thermally stable resins, optical coatings, or dielectric materials [52, 53].

3.4 Antimicrobial activity

The antimicrobial potency of PHS and its derivatives (ES1, ES2, ES3 and ES4) against Gram-positive bacteria (*S. aureus* (*ATCC25923)* and *B. subtilis (ATCC 6633)*), Gram-negative bacteria (*E. coli 0157 (KY797670)* and *K. pneumonia (ST627*) and the fungal strain (*C. albicans (ATCC 10231*) was assessed using the agar well diffusion technique. The results were shown in Fig. 7. The derivatives exhibited a varied range of inhibition effects based on the impact of the investigated derivatives on the microorganism. ES3 and ES4 had the greatest inhibitory effect against *S. aureus*, surpassing the PHS. Conversely, ES1 and ES2 exhibited sufficient action, suggesting that particular structural alterations augment antibacterial efficacy [54]. This observation supports with previous studies that refer to the drivatives of aminophosphate can increase membrane permeability so enhancing antibacterial action [55]. *B. subtilis* presented high sensitivity to ES1 and ES4, recording an inhibition zone of roughly 40 mm, while ES2 and ES3 demonstrated adequate effects. Against this strain, the origin polymer exhibited the least effect of inhibition. The significant antibacterial activity of ES1 and ES4 attributed to their enhanced interaction with bacterial cell membranes, leading to increased permeability and disruption of cellular integrity [56]. Statistical analysis showed significant differences in inhibition zones between the derivatives ($p<0.05$) as shown in Fig. 8. While *E. coli*, resistance was observed for most derivatives except ES1. This resistance is attributed to the outer membrane of Gram-negative bacteria, especially *E. coli*, which acts as a barrier to many antimicrobial agents. The relatively low activity against *E. coli* supports by the previous study [57]. *K. pneumoniae* showed the highest susceptibility to ES1 and ES4, whereas ES2 and ES3 exhibited lower inhibitory effects. In contrast, *C. albicans* showed moderate sensitivity to ES1 and ES4, while ES2 and ES3 showed minimal antifungal activity. The minimum inhibitory concentration (MIC) of the compounds was determined and is presented in Fig. 9. ES1 and ES4 showed the lowest MIC values against most tested microorganisms, highlighting their potent antimicrobial properties. In contrast, ES2 and ES3 required higher concentrations to achieve inhibition. The presence of standard error bars in Fig. 8 reflects the variability observed in three independent experiments. Our study demonstrated that the PHS and its derivatives (ES1, ES2, ES3 and ES4) exhibited broad-spectrum antimicrobial action against both types of tested bacterial strains, as well as fungi. The greater susceptibility of Gram-positive bacteria, including *Staphylococcus aureus* and *Bacillus subtilis*, compared to Gram-negative bacteria such as *Escherichia coli* and *Klebsiella pneumonia* [58, 59]. This difference is likely due to the thick peptidoglycan layer in Gram-positive

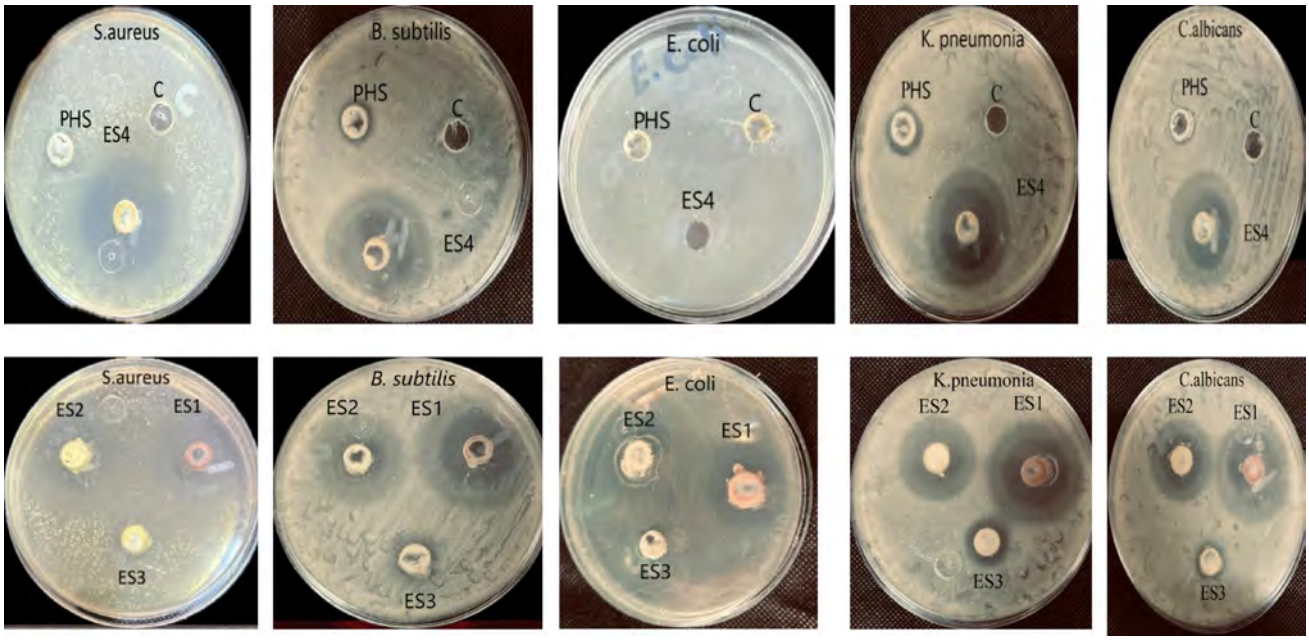

Fig. 7 Antimicrobial Activity of PHS and its derivatives ES1, ES2, ES3 and ES4 against *(S. aureus), (B.subtilis), (E.coli), (K.pneumonia)* and *(C. albicans)* and **C** represent Control (DMSO)

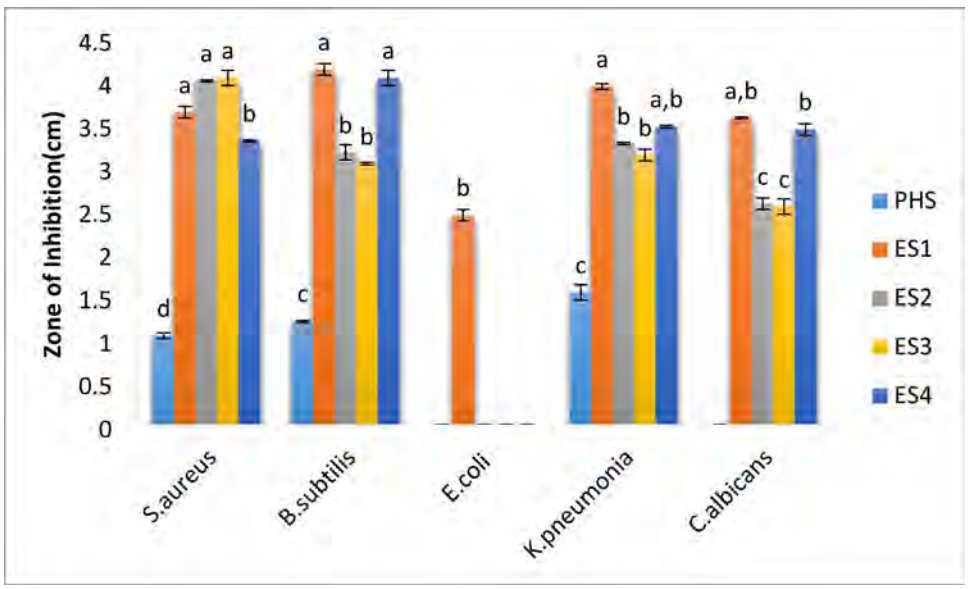

Fig. 8 Antimicrobial Activity of PHS and its derivatives ES1, ES2, ES3 and ES4 against *(S. aureus), (B.subtilis), (E.coli), (K.pneumonia)* and *(C.albicans)*. a, b, c, d Statistical significant difference ($P<0.05$) a>b>c>d

bacteria, which is more easily penetrated by its derivatives compared to the outer membrane barrier of Gram-negative bacteria [60]. To better contextualize the antimicrobial performance of the synthesized α-aminophosphonate derivatives (ES1-ES4), a comparative discussion with previously reported antimicrobial polymers has been included. Prior studies on cationic and phosphonium-based systems [59] have reported MIC values within the microgram range against Gram-positive and Gram-negative organisms, indicating high potency of such functionalized polymers. In the present work, the synthesized derivatives exhibited notable antimicrobial activity at a considerably low concentration range. ES2 and ES4 demonstrated MIC values down to 0.625 µg/mL against *S. aureus*, while maintaining activity against *E. coli* and *K. pneumoniae* at similarly low levels. These results indicate that the antibacterial activity of our derivatives is comparable to several established antimicrobial polymeric systems [28]. This improved potency may be attributed to the incorporation of phenyl-phosphonate moieties, which enhance electrostatic attraction and hydrophobic interactions with microbial cell membranes, promoting higher permeability and impairing cell integrity. The

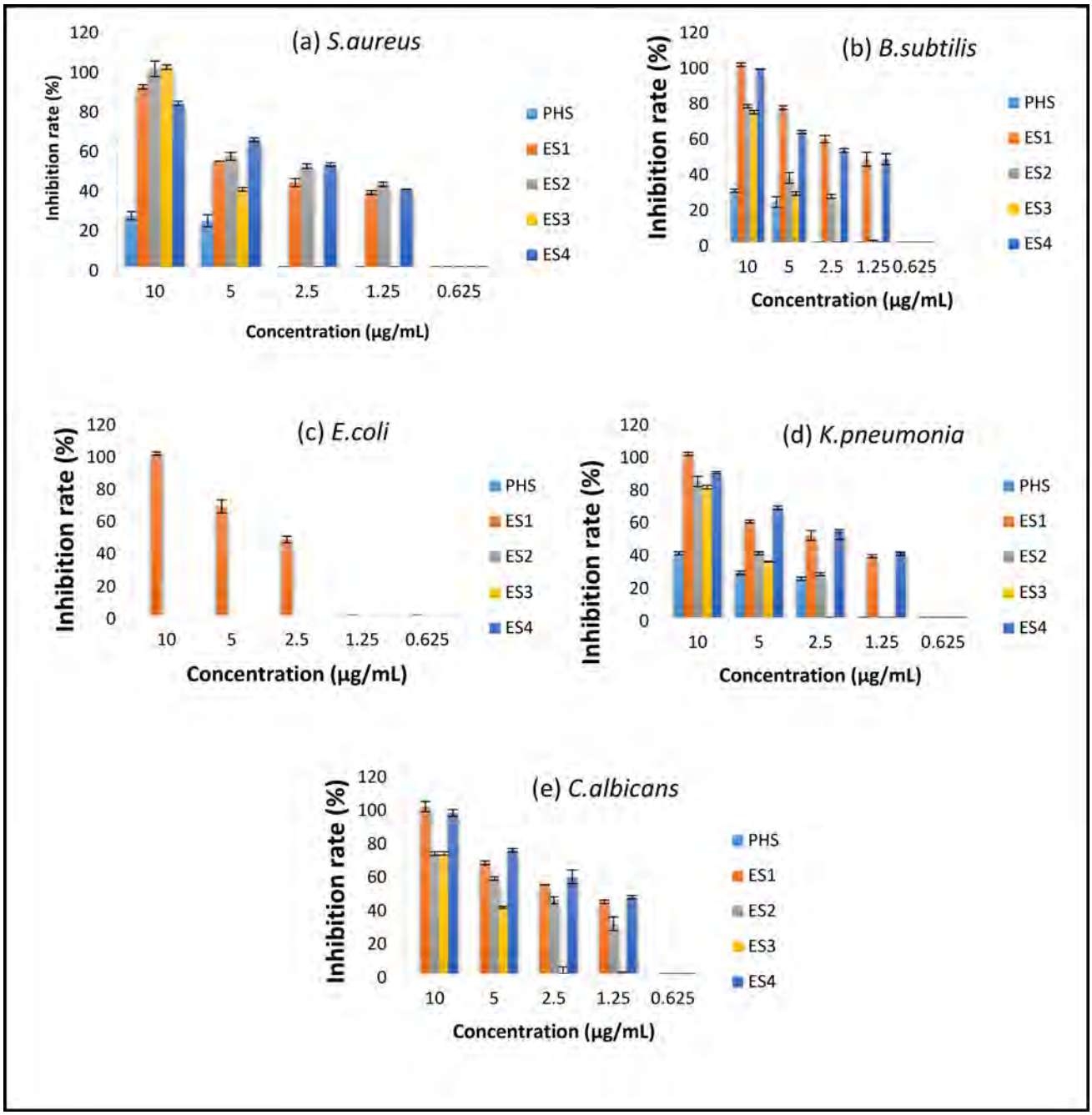

Fig. 9 MIC of PHS and its derivatives ES1, ES2, ES3 and ES4 against **a***Staphylococcus aureus (S. aureus)*,**b***Bacillus subtilis (B.subtilis)*,**c***Escherichia coli (E.coli)*,**d***Klebsiella pneumonia (K.pneumonia)* and **e***Candida albicans (C.albicans)* with standard error bars. Concentrations are expressed in µg/mL

observed variations in antibacterial performance can be attributed to the structural and electronic differences among the derivatives [60]. The superior potency of ES2 may be linked to the strong electron-withdrawing influence of the para-chloro substituent, which enhances electrostatic interaction and facilitates membrane disruption [61]. The moderate enhancement displayed by ES3 and ES4 is likely due to the electron-donating methoxy and hydroxyl substituents, which promote hydrogen-bonding affinity with microbial surfaces [62]. These findings demonstrate a clear structure–activity relationship where substituent-induced electronic modulation plays a key role in optimizing antibacterial efficacy among the synthesized α-aminophosphonate polymers [63]. The higher antibacterial activity observed for ES2 and ES4, particularly against *S. aureus* and *B. subtilis*, is consistent with the electronic structure variations revealed

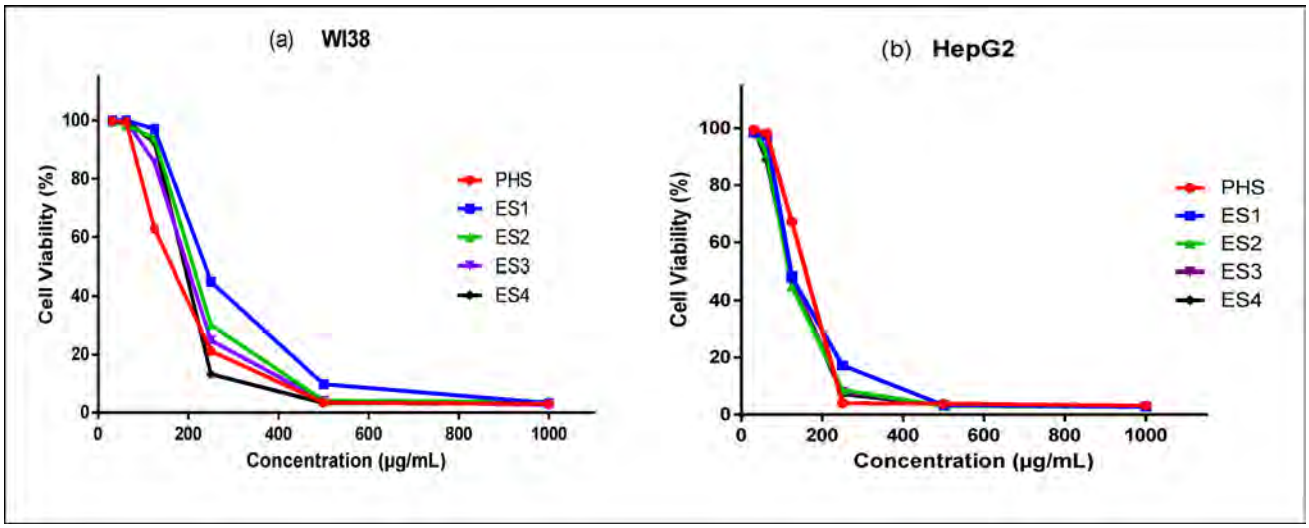

Fig. 10 Cytotoxic Effect of (PHS, ES1, ES2, ES3 and ES4) at various concentrations on a) WI38 (normal human fibroblast) and b) HepG2 (human liver cancer) cell lines

Table 4 IC_{50} values and Selectivity Index of the parent compound and its derivatives against WI38 and HepG2 cell lines

Samples	Calculated IC_{50} (µg/mL)		Selectivity index (SI)*
	WI38	HepG2	
PHS	172.73 ± 1.15	158.55 ± 4.33	1.09
ES1	236.54 ± 3.22	155.18 ± 2.46	1.52
ES2	203.95 ± 1.60	118.27 ± 0.90	1.72
ES3	193.38 ± 2.14	121.75 ± 1.13	1.59
ES4	181.37 ± 0.88	121.18 ± 1.00	1.50

*Selectivity Index (SI) = IC_{50} value in normal cells (WI38) / IC50 value in cancer cells (HepG2)

through TD-DFT analysis. ES2 demonstrated the highest electron delocalization and the most favorable polymer–solvent interaction parameters (high dn/dc and positive A2 values), which facilitate stronger electrostatic attraction and improved accessibility to microbial membranes. In contrast, ES1 exhibited lower solubility and more restricted charge distribution, supporting with its reduced antimicrobial performance. These results indicate that functional group-dependent electronic modulation directly influences bacterial susceptibility, confirming a strong structure–activity relationship.

3.5 Cytotoxicity evaluation using MTT assay

The cytotoxicity assessment of the original polymer (PHS) and its synthesized derivatives (ES1, ES2, ES3 and ES4) was evaluated against normal human lung fibroblast cells (WI38) and human liver cancer cells (HepG2) using the MTT assay. The findings showed preliminary cytotoxic effects across all tested polymer as shown in Fig. 10. In WI38 normal cells, the IC_{50} values ranged from 172.73 ± 1.15 to 236.54 ± 3.22 µg/mL (Table 4). The original polymer showed an IC_{50} of 172.73 ± 1.15 µg/mL, while ES1 exhibited the highest IC_{50} value (236.54 ± 3.22 µg/mL), refer to lower toxicity toward normal cells. Derivatives ES2, ES3 and ES4 demonstrated intermediate IC_{50} values of 203.95 ± 1.6, 193.38 ± 2.14 and 181.37 ± 0.88 µg/mL, respectively.

A noticeable difference in cell response was observed within the lower concentration range, where HepG2 cells showed a more pronounced decrease in viability compared with normal fibroblasts. This behavior suggests a degree of preferential interaction with cancer cell membranes at sub-toxic doses, supporting the classification of these materials as having potential selectivity rather than clear-cut anticancer action (Table 4). Therefore, the interpretation has been refined to emphasize the promising behavior observed at lower dosages. These results showed that the synthesized derivatives, particularly ES1, have safety profiles compared to the original compound on normal cells [64, 65]. On the other hand, the polymeric derivatives established enhanced cytotoxic activity against HepG2 cancer cells with IC_{50} values ranging from 118.27 ± 0.9 to 158.55 ± 4.33 µg/mL (Table 4). The origin PHS showed an IC_{50} of 158.55 ± 4.33 µg/mL, while ES2, ES3 and ES4 exhibited significantly lower IC_{50} values of 118.27 ± 0.9, 121.75 ± 1.13 and 121.18 ± 1 µg/mL, respectively. This recommends that these derivatives possess improved anticancer potential compared to the origin polymer. ES1 showed an IC_{50} value (155.18 ± 2.46 µg/mL) similar to the origin polymer. The selectivity index (SI) (Table 4), calculated as the ratio of IC_{50} values between normal and cancer cells, indicated that the synthesized derivatives established enhanced selective cytotoxicity toward cancer cells compared to normal cells. ES2 showed the highest selectivity with an SI of 1.72, followed by ES3 (1.59) and ES4 (1.50), while the origin PHS

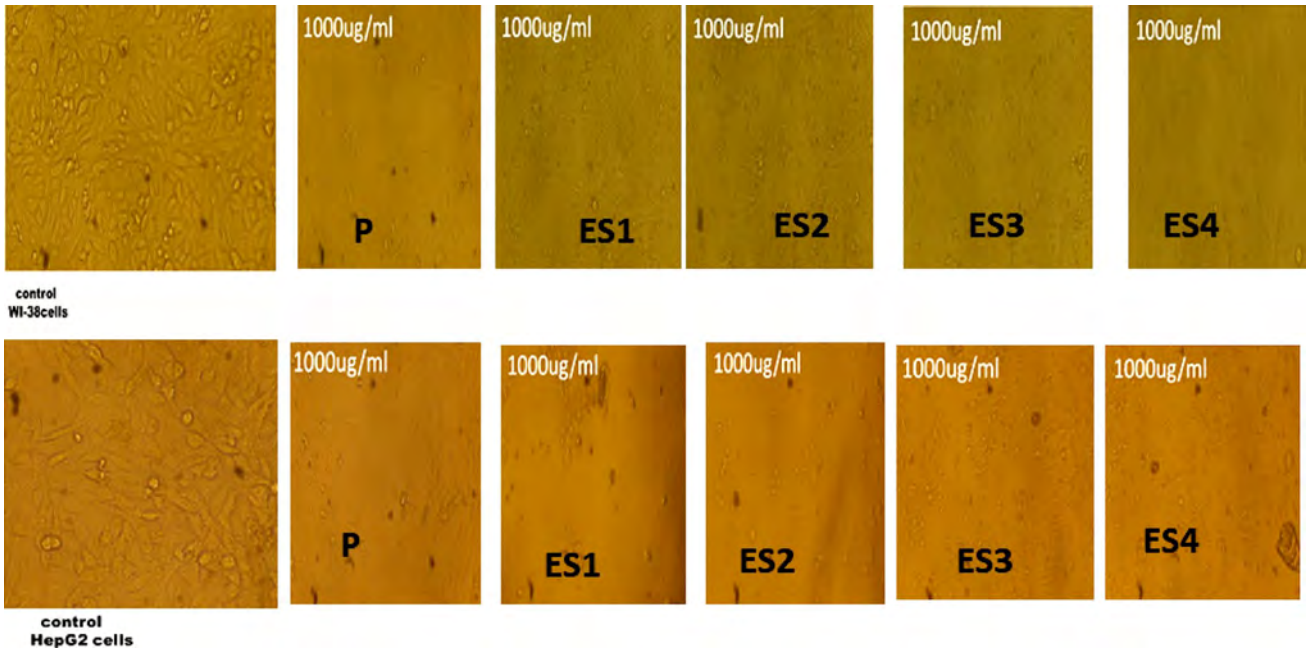

Fig. 11 Morphological changes in Wi38 and HepG2 cells treated with compounds HPS and ES1-ES4 at 1000 µg/mL. Representative microscopic images showing the effect of parent compound (PHS) and its derivatives (ES1-ES4) on cell morphology of normal lung fibroblasts (Wi38) and liver cancer cells (HepG2) after 24 h of treatment

and ES1 showed lower selectivity indices of 1.09 and 1.52, respectively [66]. At higher concentrations (500–1000 µg/mL), all compounds showed significant cytotoxicity in both cell lines, with cell viability dropping below 5% (However, at lower concentrations (31.25–62.5 µg/mL), the compounds maintained cell viability above 90% in normal cells while showing moderate cytotoxicity in cancer cells, particularly for derivatives ES2, ES3 and ES4 [65]. The higher anticancer potential of aminophosphate ES2 drivative, which contains 4-chlorobenzaldehyde moiety, suggests that the electron-withdrawing chloro substituent at the para position enhances interaction with cancer cell targets [67]. Similarly, the presence of electron-donating groups in ES3 (4-methoxybenzaldehyde) and ES4 (4-hydroxybenzaldehyde) also contributed to improved anticancer activity compared to the origin compound [68]. Our study represented that the structural modifications introduced in derivatives ES2, ES3 and ES4 successfully enhanced their anticancer potential while maintaining relatively lower toxicity toward normal cells. The improved selective cytotoxicity of these derivatives makes them promising candidates for further investigation as anticancer agents. A similar correlation was evident in the cytotoxicity profile. ES2, which showed the greatest electron delocalization and the lowest glass transition temperature, also exhibited the lowest IC_{50} value against HepG2 cells. The greater molecular flexibility likely enables enhanced cellular uptake and interaction with cancer cell components, explaining the more pronounced reduction in cell viability. Conversely, the relatively higher rigidity and localized charge distribution observed in ES1 are consistent with its weaker cytotoxic behavior. These correlations demonstrate that electronic structure and physicochemical properties predicted by DFT calculations can serve as strong indicators of biological performance.

3.6 Cell morphological alterations caused by tested compound

Microscopic evaluation was performed to monitor dose-dependent morphological changes following exposure to the synthesized compounds at different concentrations (31.25, 62.5, 125, 250, 500, and 1000 µg/mL). As presented in Fig. 11, representative images at 1000 µg/mL demonstrated noticeable alterations in HepG2 cancer cells, including rounding, reduced confluency, and weakened attachment to the culture surface. Wi38 normal cells showed milder changes at the same concentration, maintaining a relatively typical fibroblast-like appearance. Detailed morphological responses across the full concentration range are provided in Supplementary Figure S1, where the alterations were found to be gradual and dose-dependent. Minimal changes were observed at $\leq$62.5 µg/mL, whereas more pronounced disruption was evident at $\geq$125 µg/mL, particularly in HepG2 cells. These qualitative observations support the quantitative patterns obtained by the MTT assay, confirming an increased loss of cellular integrity with increasing exposure dose [69].

4 Conclusion

This study illustrated the successful synthesis and characterization of new α-aminophosphonate (ES1-ES4) derived from poly(*p*-hydroxystyrene) through chloroacetylation, amination and aminophosphate production methods. The chemical structures of these derivatives were thoroughly validated using FTIR, NMR spectroscopy and thermal analysis. Thermal study demonstrated that the inclusion of aminophosphonate groups markedly modified the thermal properties of the polymer, with ES3 displaying the greatest thermal stability among the derivatives, maintaining 32% of its weight after degradation. Static laser light scattering tests yielded significant insights into the molecular properties of the produced derivatives. The significant increases in molecular weight, radius of gyration and second virial coefficient relative to the pristine polymer further validated the effective alteration. ES2 demonstrated the highest refractive index increment (3.2662 mL/g). The computational research employing DFT simulations elucidated significant electronic and structural characteristics of the derivatives. Antimicrobial testing revealed that the polymers had remarkable effect against various pathogens. ES1 and ES4 had the most potent antibacterial activity, demonstrating superior efficacy against Gram-positive bacteria compared to Gram-negative bacteria. The results of the (MIC) corroborated these observations. Cytotoxicity experiments indicated that all derivatives exhibited reduced toxicity towards normal cells (WI38) in comparison to cancer cells (HepG2). ES2 exhibited the highest selectivity index (1.72), signifying the optimal equilibrium between anticancer efficacy and safety. Microscopic analysis demonstrated that the derivatives elicited more significant morphological alterations in cancer cells compared to normal cells, hence corroborating their selective toxicity. This research concludes that α-aminophosphonate derivatives of poly(p-hydroxystyrene) are attractive candidates for advanced materials exhibiting multifunctional features, such as antibacterial activity and anticancer uses.

Supplementary Information The online version contains supplementary material available at https://doi.org/10.1007/s13233-025-00475-7.

Author contributions Esraa M. El-nshar: Conceptualization, Methodology, Validation, Investigation, Data Curation, Writing–Original Draft, Visualization. El-Refaie Kenawy: Resources, Writing–Review and Editing Wesam E Yousuf: Conceptualization, Methodology, Validation, Investigation, Data Curation, Writing–Original Draft, Visualization. Ahmed R. Ghazy: Methodology, software, Validation, Investigation, Data Curation, Writing–Original Draft, Visualization. Kamal I. Aly: Resources, Writing–Review and Editing. Samar A. Khattab: Conceptualization, Methodology, Validation, Investigation, Data Curation, Writing–Original Draft, Visualization.

Funding Open access funding provided by The Science, Technology & Innovation Funding Authority (STDF) in cooperation with The Egyptian Knowledge Bank (EKB). Not applicable.

Data availability The authors affirm that the article contains all of the data created or examined during this investigation.

Declarations

Conflict of interest There is no conflict of interest.

References

1. I. Kraicheva, A. Bogomilova, I. Tsacheva, G. Momekov, D. Momekova, K. Troev, Synthesis, NMR characterization and in vitro cytotoxicity evaluation of new poly(oxyethylene aminophosphonate)s. Eur. J. Med. Chem. **45**(12), 6039–6044 (2010). https://doi.org/10.1016/j.ejmech.2010.10.002
2. E.A. Imam, A.I. Hashem, A.A. Tolba, M.G. Mahfouz, I.E.T. El-Sayed, A.I. El-Tantawy, E. Guibal, Effect of mono-vs. bi-functionality of aminophosphonate derivatives on the enhancement of U (VI) sorption: physicochemical properties and sorption performance. J. Environ. Chem. Eng. **11**(3), 109951 (2023). https://doi.org/10.1016/j.jece.2023.109951
3. P. Canepa, G. Gonella, G. Pinto, V. Grachev, M. Canepa, O. Cavalleri, Anchoring of aminophosphonates on titanium oxide for biomolecular coupling. J. Phys. Chem. C **123**(27), 16843–16850 (2019). https://doi.org/10.1021/acs.jpcc.9b04077
4. S. Poreddy, M. Gundluru, S. Sarva, S. Pothuraju, P. Bellala, K.K. Konidala, S.R. Cirandur, Eco-friendly synthesis, antimicrobial activity, molecular docking and ADMET studies of novel α-aminophosphonates. Org. Commun. **17**(3), 144–165 (2024). https://doi.org/10.25135/acg.oc.172.24.07.3269
5. G.L. Samia, A. Karima, H. Fares, B. Houda, H. Sihem, T. Bouteina, S. Amel, Synthesis, characterization, antibacterial activity, DFT and molecular docking studies of four4-phenyldiazenyl phenyl aminophosphonates. J. Mol. Struct. **1309**, 138181 (2024). https://doi.org/10.1016/j.molstruc.2024.138181
6. I. Bazine, Z. Cheraiet, R. Bensegueni, C. Bensouici, A. Boukhari, Synthesis, antioxidant and anticholinesterase activities of novel quinoline-aminophosphonate derivatives. J. Heterocycl. Chem. **57**(5), 2139–2149 (2020). https://doi.org/10.1002/jhet.3933
7. N. Chafai, O. Moumeni, S. Chafaa, Novel α-aminophosphonate derivates synthesis, theoretical calculation, molecular docking, and in silico prediction of potential inhibition of SARS-CoV-2. J. Mol. Struct. **1272**, 134196 (2023). https://doi.org/10.1016/j.molstruc.2022.134196
8. R. Bahadi, M. Berredjem, C. Benzaid, F. Bouchareb, A. Dekir, M.L. Djendi, R. Redjemia, Efficient synthesis, crystallography

study, antibacterial/antifungal activities, DFT/ADMET studies and molecular docking of novel α-aminophosphonates. J. Mol. Struct. **1289**, 135849 (2023). https://doi.org/10.1016/j.molstruc.2023.135849
9. Z. Rezaei, H. Firouzabadi, N. Iranpoor, A. Ghaderi, M.R. Jafari, A.A. Jafari, H.R. Zare, Design and one-pot synthesis of α-aminophosphonates and bis (α-aminophosphonates) by iron (III) chloride and cytotoxic activity. Eur. J. Med. Chem. **44**(11), 4266–4275 (2009). https://doi.org/10.1016/j.ejmech.2009.07.009
10. Q. Ran, J. Ma, T. Wang, H. Zhao, F. Song, S. Fan, J. Liu, Synthesis, characterization and dispersion properties of a series of bis (phosphonic acid) amino-terminated polymers. Colloid Polym. Sci. **294**(1), 189–198 (2016). https://doi.org/10.1007/s00396-015-3734-1
11. H.M.S. Al-Jubori, T.S.F. Al-Mathkuri, Z.R. Banoon, M.Y. Saleh, Synthesis of novel benzo [d] imidazole bearing α-aminophosphonate and their antimicrobial evaluation. Results Chem. **8**, 101586 (2024). https://doi.org/10.1016/j.rechem.2024.101586
12. A.K. Mungara, Y.K. Park, K.D. Lee, Synthesis and antiproliferative activity of novel α-aminophosphonates. Chem. Pharm. Bull. **60**(12), 1531–1537 (2012)
13. E.R.S. Kenawy, M.M. Azaam, K.M. Saad-Allah, Synthesis and antimicrobial activity of α-aminophosphonates containing chitosan moiety. Arab. J. Chem. **8**(3), 427–432 (2015). https://doi.org/10.1016/j.arabjc.2013.12.029
14. M.E. El-Naggar, A.M. Abdelgawad, T.I. Shaheen, S.A. El-Kholy, M.M. Hashem, D.A. Elsherbiny, Viable approach for preventing skin wound infections using bioactive dressing films from chitosan-furfural/α-aminophosphonate nanocomposite. Int. J. Biol. Macromol. **306**(Pt 3), 141731 (2025). https://doi.org/10.1016/j.ijbiomac.2025.141731
15. F.A. Alasmary, E.R. Kenawy, N.M. El-Deeb, E.A. Kamoun, S.A. Khattab, A.M. Karami, M.M. Azaam, Synthesis, antimicrobial and anticancer activities of Tetronic 1107 Schiff bases. Polym. Adv. Technol. **33**(9), 2787–2797 (2022). https://doi.org/10.1002/pat.5732
16. E.R. Kenawy, A.E.R.R. El-Shanshoury, N. Omar Shaker, B.M. El-Sadek, A.H. Khattab, A. Elzatahry, Synthesis and biocide activity of polymers based on poly(hydroxy styrene) and poly(hydroxy styrene-co-2-hydroxyethyl methacrylate). Main Group Chem. **12**(4), 293–306 (2013). https://doi.org/10.3233/MGC-130109
17. E.R. Kenawy, A.E.R.R. El-Shanshoury, N. Omar Shaker, B.M. El-Sadek, A.H. Khattab, B. Ismail Badr, Biocidal polymers: synthesis, antimicrobial activity, and possible toxicity of poly (hydroxystyrene-co-methylmethacrylate) derivatives. J. Appl. Polym. Sci. **120**(5), 2734–2742 (2011). https://doi.org/10.1002/app.33046
18. E.R. Kenawy, S.H. El-Khalafy, H.A. Abosharaf, E.M. El-nshar, A.R. Ghazy, M.M. Azaam, Synthesis, characterization, and anticancer potency of branched poly (*p*-Hydroxy Styrene) Schiff-Bases. Macromol. Biosci. **23**(11), 2300090 (2023). https://doi.org/10.1002/mabi.202300090
19. S.H. El-Khalafy, M.M. Azaam, E.M. El-nshar, E.A. Kamoun, E.R. Kenawy, Catalytic activity of Co (II)-porphyrin anchored onto polymeric support of electrospun polyacrylonitrile nanofiber: synthesis and efficient green oxidation of crystal violet dye with hydrogen peroxide. Biomass Conversion Biorefin. **15**(1), 775–786 (2025). https://doi.org/10.1007/s13399-023-05073-0
20. C. Erhonyota, G.I. Edo, F.O. Onoharigho, Comparison of poison plate and agar well diffusion method determining the antifungal activity of protein fractions. Acta Ecol. Sin. **43**(4), 684–689 (2023). https://doi.org/10.1016/j.chnaes.2022.08.006
21. P.K. Mishra, S. Mishra, G. Selvakumar, S.C. Bisht, J.K. Bisht, S. Kundu, H.S. Gupta, Characterisation of a psychrotolerant plant growth promoting *Pseudomonas* sp. strain PGERs17 (MTCC 9000) isolated from North Western Indian Himalayas. Ann. Microbiol. **58**, 561–568 (2008). https://doi.org/10.1007/BF03175558
22. R. Rahmayanti, Z. Zildiya, & C. A. Nuraskin. Isolation of the fungi candida albicans in teenage girls urine using sabouraud dextrose agar (SDA) Media. In AICH: Aceh International Conference on Health (Vol. 1, No. 2) (2024) https://doi.org/10.30867/aich.v1i2.731
23. D.D.C.F. Bruno, T.F. Bartelli, C.R. Rodrigues, M.R. Briones, Prolonged growth of *Candida albicans* reveals co-isolated bacteria from single yeast colonies. Infect. Genet. Evol. **65**, 117–126 (2018). https://doi.org/10.1016/j.meegid.2018.07.021
24. O.R. Adeoyo, B.I. Pletschke, J.F. Dames, Molecular identification and antibacterial properties of an ericoid associated mycorrhizal fungus. BMC Microbiol. **19**, 1–8 (2019). https://doi.org/10.1186/s12866-019-1555-y
25. S. Agrawal, C.J. Barrow, S.K. Deshmukh, Structural deformation in pathogenic bacteria cells caused by marine fungal metabolites: an in vitro investigation. Microb. Pathog. **146**, 104248 (2020). https://doi.org/10.1016/j.micpath.2020.104248
26. A. Chhetri, M. Paudel, T. R. Gompo, & S. Thapaliya (2024). Study on minimum inhibitory concentration of selected antibacterials against bacterial isolates from canine pyometra. https://doi.org/10.20944/preprints202408.1339.v1
27. P. Parvekar, J. Palaskar, S. Metgud, R. Maria, S. Dutta, The minimum inhibitory concentration (MIC) and minimum bactericidal concentration (MBC) of silver nanoparticles against *Staphylococcus aureus*. Biomater. Investig. Dent. **7**(1), 105–109 (2020). https://doi.org/10.1080/26415275.2020.1796674
28. M. Venkatesh, V.A. Barathi, E.T.L. Goh, R. Anggara, M.H.U.T. Fazil, A.J.Y. Ng, R. Lakshminarayanan, Antimicrobial activity and cell selectivity of synthetic and biosynthetic cationic polymers. Antimicrob. Agents Chemother. **61**(10), 10–1128 (2017). https://doi.org/10.1128/aac.00469-17
29. X. Huang, M. Wang, C. Wang, W. Hu, Q. You, T. Ma, H. Wang, Synthesis and biological evaluation of novel millepachine derivative containing aminophosphonate ester species as novel antitubulin agents. Bioorg. Chem. **94**, 103486 (2020). https://doi.org/10.1016/j.bioorg.2019.103486
30. G. Gnanamoorthy, T. Dhanasekaran, S. Munusamy, A. Padmanaban, A. Stephen, V. Narayanan, Photocatalytic and biological properties of porous titanium aminophosphate. Appl. Nanosci. **8**, 1791–1807 (2018). https://doi.org/10.1007/s13204-018-0855-0
31. M. Rajabzadeh, Z. Fekrirad, M. Jalali Nadoushan, I. Rasooli, Characterizing the interplay between *Acinetobacter baumannii*, A549 cells, and anti-Omp34 antibodies: implications for adherence, internalization, and cytotoxicity. Folia Microbiol. **70**(3), 1–11 (2024). https://doi.org/10.1007/s12223-024-01218-4
32. A. Ulu, S.K. Sezer, Ş Yüksel, A. Koç, B. Ateş, Preparation, controlled drug release, and cell viability evaluation of tenofovir alafenamide-loaded chitosan nanoparticles. Starch-Stärke **76**(1–2), 2100144 (2024). https://doi.org/10.1002/star.202100144
33. E.H. Wong et al., Modulating antimicrobial activity and mammalian cell biocompatibility with glucosamine-functionalized star polymers. Biomacromol **17**(3), 1170–1178 (2016). https://doi.org/10.1021/acs.biomac.5b01766
34. R.M. Humphries et al., CLSI methods development and standardization working group best practices for evaluation of antimicrobial susceptibility tests. J. Clin. Microbiol. (2018). https://doi.org/10.1128/jcm.01934-17
35. S. El-Kalyoubi, S.A. El-Sebaey, A.M. Rashad, H.A. Al-Ghulikah, M.M. Ghorab, S.M. Elfeky, Synthesis, DFT calculations, and anti-proliferative evaluation of pyrimidine and selenadiazolopyrimidine derivatives as dual Topoisomerase II and HSP90 inhibitors. J. Enzyme Inhib. Med. Chem. **38**(1), 2198163 (2023). https://doi.org/10.1080/14756366.2023.2198163

36. D. Cavallo, P. Chiarella, A.M. Fresegna, A. Ciervo, V. Del Frate, C.L. Ursini, Metal oxide nanoparticles and graphene-based nanomaterials: genotoxic, oxidative, and epigenetic effects. Impact Eng. Nanomater. Genomics Epigenom. (2023). https://doi.org/10.1002/9781119896258.ch5
37. R.R. Neiber, N.A. Samak, J. Xing, E.I. Elmongy, A.A. Galhoum, I.E.T. El Sayed, X. Lu, Synthesis and molecular docking study of α-aminophosphonates as potential multi-targeting antibacterial agents. J. Hazard. Mater. **465**, 133203 (2024). https://doi.org/10.1016/j.jhazmat.2023.133203
38. A.J. Rao, P.V. Rao, V.K. Rao, C. Mohan, C.N. Raju, C.S. Reddy, Microwave assisted one-pot synthesis of novel α-aminophosphonates and their biological activity. Bull. Korean Chem. Soc. **31**(7), 1863–1868 (2010). https://doi.org/10.5012/bkcs.2010.31.7.1863
39. S.S. Reddy, V.K. Rao, B.S. Krishna, C.S. Reddy, P.V. Rao, C.N. Raju, Synthesis, antimicrobial, and antioxidant activity of new α-aminophosphonates. Phosphorus Sulfur Silicon Relat. Elem. **186**(7), 1411–1421 (2011). https://doi.org/10.1080/10426507.2010.514682
40. K. Benbouguerra, S. Chafaa, N. Chafai, M. Mehri, O. Moumeni, A. Hellal, Synthesis, spectroscopic characterization and a comparative study of the corrosion inhibitive efficiency of an α-aminophosphonate and Schiff base derivatives: experimental and theoretical investigations. J. Mol. Struct. **1157**, 165–176 (2018). https://doi.org/10.1016/j.molstruc.2017.12.049
41. E.R. Kenawy, F. Abdel-Hay, M. El-Newehy, E.H. Abd El-Zaher, E.M. Abo-Elghit Ibrahim, Novel biocidal polymers based on branched and linear poly (hydroxystyrene). Int. J. Polym. Mater. Polym. Biomater. **65**(14), 712–719 (2016). https://doi.org/10.1080/00914037.2016.1163563
42. A.S. Morshedy, A.A. Galhoum, A.A.H.A. Aleem, M.T.S. El-din, D.M. Okaba, M.S. Mostafa, I. ET-El-Sayed, Functionalized aminophosphonate chitosan-magnetic nanocomposites for Cd (II) removal from aqueous solutions: performance and mechanisms of sorption. Appl. Surf. Sci. **561**, 150069 (2021). https://doi.org/10.1016/j.apsusc.2021.150069
43. B. El-Baradie, R. Ghazy, A. El-Shaer, F. El-Mekawey, Optical selection of the preferred solvent of a standard polymer for laser light scattering phenomena investigations. Phys. B Condens. Matter **292**(3–4), 208–212 (2000). https://doi.org/10.1016/S0921-4526(00)00473-7
44. R. Ghazy, N. Fotoh, B. Moharam, F. El-Mekawey, On physics of optical laser light scattering (OLLS) of an industrial polymer which may assist in physics of random laser (RL) investigation. J. Light. Vis. Environ. **33**(1), 24–36 (2009). https://doi.org/10.2150/jlve.33.24
45. T. Tumolo, L. Angnes, M.S. Baptista, Determination of the refractive index increment (dn/dc) of molecule and macromolecule solutions by surface plasmon resonance. Anal. Biochem. **333**(2), 273–279 (2004). https://doi.org/10.1016/j.ab.2004.06.010
46. R. Ghazy, B. El-Baradie, A. El-Shaer, F. El-Mekawey, Measurements of the refractive indices and refractive index increment of a synthetic PMMA solutions at 488 nm. Opt. Laser Technol. **31**(5), 335–340 (1999). https://doi.org/10.1016/S0030-3992(99)00065-1
47. R. Ghazy, Determination of scattering parameters of a new copolymer by using a laser scattering method. Am. J. Appl. Sci. **8**(6), 603 (2011)
48. M.E. Shaheen, A.R. Ghazy, E.R. Kenawy, R.A. Ghazy, F. El-Mekawy, Experimental studies on static laser light scattering of synthetized poly (acrylonitrile-co-methyl methacrylate) copolymer at room temperature. Optik **224**, 165773 (2020). https://doi.org/10.1016/j.ijleo.2020.165773
49. A.R. Ghazy, M.M. El-Sheekh, R. Ghazy, Structure, laser scattering, optical properties, adsorption, and dye removal studies by Ulvan extracted from the green seaweed *Ulva lactuca*. J. Mol. Liq. **410**, 125567 (2024). https://doi.org/10.1016/j.molliq.2024.125567
50. P. Debye, Light scattering in solutions. J. Appl. Phys. **15**(4), 338–342 (1944). https://doi.org/10.1063/1.1707436
51. A.R. Ghazy, O.M. Hemeda, A.F. Al-Hossainy, R. Ghazy, A.M.A. Henaish, Docking of COVID-19 main protease and TD-DFT/DMOl3 simulated method, synthesis, and characterization with hybrid nanocomposite thin films and its applications. Surfaces Interfaces **37**, 102722 (2023). https://doi.org/10.1016/j.surfin.2023.102722
52. S.A.A. Gawad, R. Ghazy, S. Mansour, H. Ahmed, A.R. Ghazy, Photo-physical characteristics of janus green B in different solvents and its interaction mechanism with silver nanoparticles. J. Fluoresc. **35**(5), 1–14 (2024). https://doi.org/10.1007/s10895-024-03723-8
53. H. Lei, X. Li, J. Wang, Y. Song, G. Tian, M. Huang, D. Wu, DFT and molecular dynamic simulation for the dielectric property analysis of polyimides. Chem. Phys. Lett. **786**, 139131 (2022). https://doi.org/10.1016/j.cplett.2021.139131
54. P.D. Wakchaure, B. Ganguly, Exploring the structure, function of thiamine pyrophosphate riboswitch, and designing small molecules for antibacterial activity. WIREs RNA **14**(4), e1774 (2023). https://doi.org/10.1002/wrna.1774
55. X.C. Yang, C.M. Zeng, S.R. Avula, X.M. Peng, R.X. Geng, C.H. Zhou, Novel coumarin aminophosphonates as potential multitargeting antibacterial agents against *Staphylococcus aureus*. Eur. J. Med. Chem. **245**, 114891 (2023). https://doi.org/10.1016/j.ejmech.2022.114891
56. S. Roy, M. Halder, P. Ramprasad, S. Dasgupta, Y. Singh, D. Pal, Oxidized pullulan exhibits potent antibacterial activity against *S. aureus* by disrupting its membrane integrity. Int. J. Biol. Macromol. **249**, 126049 (2023). https://doi.org/10.1016/j.ijbiomac.2023.126049
57. A.M. Carmona-Ribeiro, L.D. de Melo Carrasco, Cationic antimicrobial polymers and their assemblies. Int. J. Mol. Sci. **14**(5), 9906–9946 (2013). https://doi.org/10.3390/ijms14059906
58. A.B. Muhammad, K. Tian, J. Park, Enhanced antimicrobial property of polyurethane fibers bearing nanoparticles of polyacrylic acid-grafted oleyl amine and zwitterion. Macromol. Res. **33**(1), 77–84 (2025). https://doi.org/10.1007/s13233-024-00316-z
59. R. Siddiqui, A. Khodja, T. Ibrahim, M. Khamis, A. Anwar, N.A. Khan, The increasing importance of novel deep eutectic solvents as potential effective antimicrobials and other medicinal properties. World J. Microbiol. Biotechnol. **39**(12), 330 (2023). https://doi.org/10.1007/s11274-023-03760-8
60. K. Chevula, P. Chennamsetti, N. Nagaraju, N. Patnam, S. Balabadra, P. Bhadraiah, V. Manga, Design synthesis of 1, 2, 3-triazoles based thiazolidine-2, 4-dione derivatives anticancer, antimicrobial, and molecular docking studies. Chem. Biodiversity (2025). https://doi.org/10.1002/cbdv.202501142
61. Y. Zborovskii, V. Orysyk, S. Orysyk, M. Vovk, Structure-activity relationship of thiourea derivatives: influence of substituents on antibacterial activity. Lett. Appl. NanoBioScience. **14**, 102 (2025)
62. L.I. Álvarez-Añorve, I. Gaugué, H. Link, J. Marcos-Viquez, D.M. Díaz-Jiménez, S. Zonszein, J. Plumbridge, Allosteric activation of Escherichia coli glucosamine-6-phosphate deaminase (NagB) in vivo justified by intracellular amino sugar metabolite concentrations. J. Bacteriol. **198**(11), 1610–1620 (2016). https://doi.org/10.1128/jb.00870-15
63. M.A. Hassan, T.M. Tamer, A.M. Omer, W.M. Baset, E. Abbas, M.S. Mohy-Eldin, Therapeutic potential of two formulated novel chitosan derivatives with prominent antimicrobial activities against virulent microorganisms and safe profiles toward

fibroblast cells. Int. J. Pharm. **634**, 122649 (2023). https://doi.org/10.1016/j.ijpharm.2023.122649
64. H.B. Kim, N. Meghani, M. Park, S.H. Lee, S.R. Lee, Y.J. Cho, K.H. Choi, Electrohydrodynamically atomized pH-responsive PLGA/ZnO quantum dots for local delivery in lung cancer. Macromol. Res. **28**(4), 407–414 (2020). https://doi.org/10.1007/s13233-020-8053-9
65. X. Huang, M. Wang, Q. You, J. Kong, H. Zhang, C. Yu, R. Huang, Synthesis, mechanisms of action, and toxicity of novel aminophosphonates derivatives conjugated irinotecan *in vitro* and *in vivo* as potent antitumor agents. Eur. J. Med. Chem. **189**, 112067 (2020). https://doi.org/10.1016/j.ejmech.2020.112067
66. M. Zahedifard, F. Lafta Faraj, M. Paydar, C. Yeng Looi, M. Hajrezaei, M. Hasanpourghadi, M. Ameen Abdulla, Synthesis, characterization and apoptotic activity of quinazolinone Schiff base derivatives toward MCF-7 cells via intrinsic and extrinsic apoptosis pathways. Sci. Rep. **5**(1), 11544 (2015). https://doi.org/10.1038/srep11544
67. M. Farouk Elsadek, B. Mohamed Ahmed, M. Fawzi Farahat, An overview on synthetic 2-aminothiazole-based compounds associated with four biological activities. Molecules **26**(5), 1449 (2021). https://doi.org/10.3390/molecules26051449
68. A.R. Kumar, L. Ilavarasan, G.S. Mol, S. Selvaraj, M. Azam, P. Jayaprakash, A. Ravi, Spectroscopic (FT-IR, FT-Raman, UV–Vis and NMR) and computational (DFT, MESP, NBO, NCI, LOL, ELF, RDG and QTAIM) profiling of 5-chloro-2-hydroxy-3-methoxybenzaldehyde: a promising antitumor agent. J. Mol. Struct. **1298**, 136974 (2024). https://doi.org/10.1016/j.molstruc.2023.136974
69. D.S. Masson-Meyers, V.V. Bumah, C.S. Enwemeka, A comparison of four methods for determining viability in human dermal fibroblasts irradiated with blue light. J. Pharmacol. Toxicol. Methods **79**, 15–22 (2016). https://doi.org/10.1016/j.vascn.2016.01.001